PP6-regulated Aurora A activity towards NDC80 limits mitotic spindle size to prevent micronucleation

Tomoaki Sobajima[1†], Katarzyna M. Kowalczyk[1†], Stefanos Skylakakis[1†], Daniel Hayward[2], Luke J. Fulcher[1], Colette Neary[1], Caleb Batley[1], Emile Roberts[2], Samvid Kurlekar[1], Ulrike Gruneberg[2], Francis A. Barr[1*]

[1]Department of Biochemistry, University of Oxford; South Parks Road; Oxford OX1 3QU

[2]Sir William Dunn School of Pathology, University of Oxford; Oxford OX1 3RE

[†]These authors contributed equally to this work

[*]Corresponding author. Email: francis.barr@bioch.ox.ac.uk

Short title: Setting a limit for mitotic spindle size

Abstract

Amplification of the mitotic kinase Aurora A or loss of its regulator protein phosphatase 6 (PP6) promote micronucleation and related nuclear structure defects, changes that have emerged as drivers of genome instability. Using functional genomics to shed light on the processes underpinning these changes, we discover synthetic lethality between PPP6C, the catalytic subunit of PP6, and the kinetochore protein NDC80. We find that during spindle formation, NDC80 is phosphorylated at microtubule-attached kinetochores carrying the PP6-regulated pool of Aurora A, and this phosphorylation persists until spindle disassembly in telophase. Expression of Aurora-phosphorylation-deficient NDC80-9A or phospho-mimetic NDC80-9D results in reduced or enlarged spindle size, respectively. PPP6C-knockout results in enlarged spindles which fail to hold chromosomes tightly together in anaphase, causing defective nuclear structure. Remarkably NDC80-9A rescues micronucleation and defective nuclear structure in these cells. These results demonstrate that NDC80 is an important target of the Aurora A-PP6 pathway and underline the importance of spindle size control for the fidelity of cell division.

Introduction

Micronucleation and related structural defects of the nucleus are emerging as important drivers for genome instability in cancers and metastasis (Bakhoum et al., 2018; Crasta et al., 2012; Zhang et al., 2015). As a consequence, there is great interest in understanding how these changes arise, and whether they expose vulnerabilities that can be exploited by new therapies. Defective chromosome segregation in mitosis has long been understood to be a cause of changes to nuclear structure (Levine and Holland, 2018). However, few of the structural or regulatory components required for chromosome segregation are mutated in cancers, and the specific molecular mechanisms going awry are often unclear and thus require further investigation. Here we focus on two regulators of mitotic spindle formation, Aurora A and the catalytic subunit of PP6, PPP6C, which are either amplified or mutated in cancers (Anand et al., 2003; Bischoff et al., 1998; Hammond et al., 2013; Hodis et al., 2012; Krauthammer et al., 2012; Sen et al., 1997).

Chromosome segregation is mediated by the mitotic spindle (Goshima and Scholey, 2010; Petry, 2016), a structure formed when microtubules emanating from the separated centrosomes at the spindle poles attach to chromosomes through a conserved protein complex at kinetochores formed by NDC80, NUF2 and SPC24/25 (Cheeseman et al., 2006; Ciferri et al., 2008; DeLuca et al., 2006). The number and length of these microtubules, and hence the formation of the mitotic spindle is tightly regulated in proportion to the number of chromosomes or amount of chromatin (Goshima and Scholey, 2010; Petry, 2016). Chromatin promotes spindle formation by the RCC1-Ran pathway, which regulates the availability of a cohort of microtubule-binding spindle assembly factors (Carazo-Salas et al., 1999; Clarke and Zhang, 2008; Heald et al., 1996; Kalab et al., 1999). Key amongst these factors is TPX2, a microtubule-binding protein and activating subunit for the mitotic kinase Aurora A that phosphorylates TPX2 and other proteins important for spindle formation, positioning and orientation (Bayliss et al., 2003; Bird and Hyman, 2008; Fu et al., 2015; Gruss et al., 2001; Gruss et al., 2002; Helmke and Heald, 2014; Kotak et al., 2016; Polverino et al., 2021). These Aurora A and TPX2 positive spindle fibers contact the kinetochores, and interestingly, TPX2 mutants unable to bind Aurora A still form short bipolar spindles that are able to segregate chromosomes (Bird and Hyman, 2008). Aurora A and TPX2 are therefore important for the formation of correctly scaled mitotic spindles, albeit the key Aurora A targets explaining this function are unclear.

This spindle assembly process is monitored by two additional kinases, Aurora B localized to centromeres and MPS1 which is dynamically recruited to kinetochores (Musacchio, 2015). Together Aurora B and MPS1 detect and initiate the checkpoint signal preventing exit from mitosis until spindle assembly is complete. MPS1 recruitment occurs at kinetochores with incorrect microtubule attachment geometries, or without attached microtubules. Microtubule binding and the generation of tension is thought to physically pull the microtubule-binding outer kinetochore proteins away from Aurora B at the centromere, thus altering their phosphorylation state. NDC80 has been reported to be phosphorylated in this context, within its N-terminal region by Aurora B, reducing microtubule-binding affinity and promoting MPS1 recruitment, spindle checkpoint signaling and chromosome biorientation (Ciferri et al., 2008; DeLuca et al., 2006; DeLuca et al., 2011; Ji et al., 2015; Zhu et al., 2013). A similar function has been proposed for Aurora A phosphorylation of NDC80 during chromosome alignment and pole-based error correction processes (Lampson and Cheeseman, 2011; Ye et al., 2015). In that case, NDC80 is phosphorylated at incorrectly positioned chromosomes overlapping with Aurora A activity at spindle poles, allowing movement of the chromosome towards the metaphase plate by other Aurora-controlled kinesin motors such as KIF4A and CENP-E (Kim et al., 2010; Poser et al., 2019).

Although the kinase activities of Aurora A and Aurora B appear to converge on some common targets such as NDC80, other evidence shows they must also have distinct functions. Inhibition of Aurora A resulting in spindle formation defects and a checkpoint-dependent arrest in mitosis, whereas inhibition of Aurora B results in loss of the checkpoint and failure to arrest in mitosis when spindle defects are present (Ditchfield et al., 2003; Hauf et al., 2003; Hoar et al., 2007). However, the specific targets of Aurora A and Aurora B that explain these differences are not clearly understood. In addition to their distinct localizations, another point of difference between Aurora A and B is in their regulation. Aurora B activity on chromosomes is controlled by the PP1-Repoman complex (Qian et al., 2015), whereas the activity of Aurora A-TPX2 complexes is limited by protein phosphatase 6 (PP6) (Zeng et al., 2010). This regulation of Aurora A is necessary for proper spindle assembly, and cancer-associated loss of function driver mutations in PPP6C, the catalytic subunit of PP6, lead to micronucleation due to defective chromosome

segregation (Hammond et al., 2013; Hodis et al., 2012; Krauthammer et al., 2012; Zeng et al., 2010). These micronuclei are positive for the DNA damage marker γ-H2AX consistent with other findings on the consequences of micronucleation and direct evidence that the loss of PPP6C is a driver for genome instability (Crasta et al., 2012; Hammond et al., 2013; Hodis et al., 2012; Krauthammer et al., 2012; Zeng et al., 2010; Zhang et al., 2015).

Despite this understanding of the importance of Aurora A and PP6 for spindle assembly and chromosome segregation, the crucial targets of Aurora A in normal cells that explain genomic instability and micronucleation when its activity is amplified remain unclear. To address this question, we used unbiased functional genomics in haploid cells to screen for genes showing positive or negative synthetic interactions with PPP6C, the catalytic subunit of PP6. This powerful approach identified the Aurora A activator TPX2 as a positive interaction, suppressing the effect of PPP6C knockout. Conversely, the gene for the kinetochore protein NDC80 showed synthetic lethality with PPP6C. This led us to explore the relationship between PP6-regulated Aurora A activity, and the Aurora B mediated phosphorylation of NDC80 previously reported to occur during spindle checkpoint signaling and pole-based error correction processes. Our data show that PP6-regulated Aurora A rather than Aurora B is the major kinase acting on NDC80, and that there is no direct function for this phosphorylation in either spindle checkpoint signaling or pole-based error correction. Instead, the PP6-regulated pool of Aurora A mediates NDC80 phosphorylation during spindle size control, and hence contributes to the formation of intact nuclei after cell division. Here, we describe these results in detail and discuss the broader implications of our work for understanding how changes in mitosis trigger genome instability and might be exploitable to kill cancer cells with specific genetic changes.

Results

Functional genomics reveals synthetic lethality between PPP6C and NDC80

We set out to identify pathways that could be targets for, and explain the effects of, amplified Aurora A activity in cells lacking PP6. To do this we performed haploid genomic screens for genes that showed synthetic growth defects with, or that suppressed PPP6C knockout (PPP6C KO). First, we established that human haploid eHAP cells were a suitable model for this approach. PPP6C KO in human haploid eHAP cells resulted in slightly slowed growth, increase in the activating pT288 phosphorylation on Aurora A and stabilization of the active kinase on metaphase and anaphase spindles, and formation of micronuclei (Fig. S1). This recapitulated the hallmarks of PP6 loss of function seen in HeLa and melanoma cell lines and confirmed they were a suitable model for loss of PP6 function (Hammond et al., 2013; Zeng et al., 2010). To allow for the difference in growth rate, equal growth time in screen 1 and equal cell divisions in screen 2 were compared (Fig. S2A-S2E). In both screens a list of core essential genes required for viability across a panel of cell lines showed negative selection (Fig. S2B and 2C). These core essential genes were similarly selected against in both the parental and PPP6C knockout cells, consistent with the idea that removal of PPP6C only affects a few specific pathways within the cell. To identify dependencies created by loss of PP6, we performed a genome-wide comparison of relative log fold-change on a per gene basis in PPP6C KO compared to parental cells. Plots of ranked log fold-change for both screens showed a similar profile of the data, with a slightly larger effect size for the equal time screen (Fig. S2D and S2E). This fits with the idea that there is a growth cost from PPP6C KO and highlights the importance of the equal cell division screen which accounts for this effect. The Aurora A activator TPX2 was amongst a very small subset of

genes showing significant, p<0.01, positive selection in PPP6C KO cells in both screens (Fig. S2F), indicating suppression of the growth defect. This agreed with the previously established relationship between these proteins (Bayliss et al., 2003), and shows this approach can identify cellular pathways relevant for understanding Aurora A function. A larger cohort of genes was found to undergo negative selection consistent with synthetic growth defects with PPP6C, including known Aurora-regulated spindle assembly factors TACC3, KIF18A/B, katanin, KIF4A (Fig. 1A). Only the kinetochore protein NDC80 and all subunits of the HUSH chromatin silencing complex underwent significant, p<0.01, negative selection in both screens (Fig. 1A). NDC80 was prioritized in subsequent work for two reasons. First, the synthetic growth defect between NDC80 and PPP6C was validated in eHAP cells using specific CRISPR gRNAs (Fig. S3). Western blots showed that NDC80 was reduced and in the case of gRNA2 truncated fragments were present (Fig. S3). To us, this suggested that PPP6C KO cells are more sensitive to the levels of NDC80 than the parental cells, indicative of a functional link between NDC80 and PP6. Second, when candidates from both screens rescreened in aneuploid HeLa cells, only NDC80 showed clearly reduced viability and pronounced nuclear morphology and growth defects after 48h in PPP6C KO compared to the parental cells (Fig. 1B and S4A). For the other candidate genes, there were less obvious growth defects and only modest increases in fragmented nuclei even at 72h suggesting they are less important than NDC80 for normal mitosis and chromosome segregation in PPP6C KO cells (Fig. S4B and S4C). The PPP6C KO HeLa cells used for these assays showed the expected increase in the activating pT288 phosphorylation on Aurora A and stabilization of the active kinase on metaphase and anaphase spindles (Fig. S5) (Hammond et al., 2013; Zeng et al., 2010). A simple explanation for discovery of NDC80 in the functional genomics screen was that either spindle checkpoint signaling or pole-based error correction were affected due to the amplified activity of Aurora A in PPP6C KO cells, and this was explored further.

The PP6-regulated pool of Aurora A is a major kinase for NDC80

NDC80 has been reported to be phosphorylated within its N-terminal region either by Aurora B to promote spindle checkpoint signaling and chromosome biorientation, or by Aurora A during chromosome alignment and pole-based error correction processes (DeLuca et al., 2006; DeLuca et al., 2011; Ji et al., 2015; Lampson and Cheeseman, 2011; Ye et al., 2015; Zhu et al., 2013). These hypotheses make testable predictions about when in mitosis and where within the cell NDC80 would be phosphorylated. In checkpoint signaling, Aurora B should phosphorylate NDC80 at unattached or non-bioriented chromosomes. For pole-based error correction, NDC80 phosphorylation would be expected predominantly at chromosomes located close to the spindle poles. To test these ideas and the specific roles of Aurora A and Aurora B, we first asked if phosphorylation of NDC80 at known Aurora consensus sites is increased in mitotic cells lacking PP6 activity (Kettenbach et al., 2011). When compared to the parental cells, Western blots revealed more NDC80 phosphorylation at S55, and a slight overall upshift in Phos-tag gels indicative of increased phosphorylation in PPP6C KO (Fig. 1C). In these PPP6C KO cells, the pT288 activating phosphorylation on Aurora A, but not the equivalent pT232 for Aurora B was elevated compared to the parental cells, suggesting the increase in NDC80 pS55 was due to Aurora A. Importantly, the antibodies used to detect Aurora A sites S55 and S62 on NDC80, reacted exclusively with phospho-specific epitopes on NDC80 (Fig. 1D). To test if elevated NDC80 phosphorylation in PPP6C KO cells was due to Aurora A, specific Aurora kinase inhibitors were used. Aurora A inhibition greatly reduced the level of NDC80 pS55 (Fig. 1E and

S6A). In contrast, specific Aurora B inhibition with two different compounds did not result in reduction of NDC80 pS55 (Fig. 1E and S6A). Examination of the respective T-loop phosphorylation on each kinase confirmed the selectivity of the different Aurora inhibitors (Fig. 1E and S6A). In PPP6C KO cells, similar results were obtained, however due to the increased steady-state level of phosphorylation due to the elevated Aurora A activity, NDC80 pS55 was reduced but not fully dephosphorylated (Fig. 1E). Crucially, PP6 does not appear to be the NDC80 phosphatase, since NDC80 was dephosphorylated with the same kinetics in parental and PPP6C KO cells treated with Aurora A inhibitor (Fig S6B and S6C). In contrast to Aurora A, ongoing Aurora B activity was not required to maintain NDC80 phosphorylation since NDC80 pS55 remained constant while Aurora B pT232 was rapidly dephosphorylated in cells treated with Aurora B inhibitors (Fig. S7D). We then asked when NDC80 phosphorylation occurred as cells passed through mitosis. NDC80 pS55 and pS62 positive kinetochores were detected from prophase to metaphase and into anaphase (Fig. 1F). This pattern was confirmed in synchronized mitotic cells exiting mitosis, which showed loss of NDC80 pS55 and upshifted NDC80 species on Phos-tag gels only in telophase (Fig. 1G). NDC80 is therefore phosphorylated throughout mitosis by Aurora A rather than Aurora B, explaining its elevated phosphorylation in PPP6C KO cells which have increased Aurora A activity.

NDC80 phosphorylation in error correction and spindle checkpoint signaling

To understand the relationship between NDC80 phosphorylation and Aurora B dependent spindle checkpoint signaling, we arrested cells with nocodazole where all kinetochores are checkpoint active, or MG132 where all kinetochores are checkpoint silenced. As expected, MPS1 localized to kinetochores in nocodazole but not MG132 treated cells, and this signal was lost when Aurora B was inhibited (Fig. 2A). Unexpectedly, there was no kinetochore signal for NDC80 pS55 in the nocodazole-arrested conditions and all kinetochores were positive for NDC80 pS55 and negative for MPS1 in checkpoint silenced MG132 arrested cells (Fig. 2A). In both nocodazole or MG132 arrested cells, Aurora B inhibition resulted in loss of the pT232 epitope marking active Aurora B, but had no effect on NDC80 pS55. This inverse relationship between checkpoint proteins and NDC80 phosphorylation was also observed for MAD1 and NDC80 pS55 (Fig. 2B). NDC80 pS55 was only detected at MAD1 negative kinetochores in both parental and PPP6C KO cells (Fig. 2C). Consistent with the biochemical data already shown (Fig. 1C), NDC80 pS55 signal was elevated at kinetochores in PPP6C KO cells, however the frequency of MAD1 positive kinetochores was not altered (Fig. 2C). Checkpoint signaling also remained Aurora B but not Aurora A sensitive in both parental and PPP6C KO cells (Fig. 3). Together these findings indicated that there were no major differences in checkpoint signaling in PPP6C KO cells, despite the altered phosphorylation of NDC80. To test if NDC80 phosphorylation occurs transiently during pole-based error correction, CENP-E inhibitor was used to trap chromosomes at spindle poles (Fig. 4A). Analysis of NDC80 pS55 showed that the level of phosphorylation was independent of chromosome position in both parental and PPP6C KO cells, but remained sensitive to Aurora A in all cases (Fig. 4B). Together, these two approaches show that NDC80 phosphorylation is mediated by Aurora A, and does not correlate with Aurora B activity, spindle checkpoint signaling or chromosome position. These data argue strongly against the possibility that amplified Aurora A activity in PPP6C KO cells takes over processes such as checkpoint signaling normally controlled by Aurora B. Together, these results suggested that Aurora A phosphorylated NDC80 at checkpoint-silenced and hence microtubule-attached kinetochores.

NDC80 phosphorylation by Aurora A at stably-attached kinetochores

To more precisely determine the relationship between NDC80 phosphorylation and microtubule-attachment state, cells were treated with the KIF11 inhibitor S-trityl L-cysteine (STLC) to create monopolar spindles with a mixture of astrin-positive microtubule-attached, and astrin-negative checkpoint-positive microtubule-free kinetochores. When stained with antibodies against astrin, a marker of attached kinetochores (Schmidt et al., 2010), these spindles display a NDC80 pS55 and pS62 were present at the subset of kinetochores positive for astrin in these monoastral spindles (Fig. 2D). We then explored the localizations of Aurora A and Aurora B relative to kinetochores during mitosis. Aurora A localized to mitotic spindle fibers that terminate at the kinetochores in both metaphase and anaphase cells (Fig. 2E and 2F) (Bird and Hyman, 2008). In contrast, Aurora B was present on the centromeres and central spindle, spatially separated from kinetochores (Fig. S7) (Carmena et al., 2012). Based on its localization, Aurora A is thus more likely to be the kinase phosphorylating NDC80 at microtubule-attached kinetochores in both metaphase and anaphase, consistent with our other biochemical data. Since PP6 is not the NDC80 phosphatase, we then asked what role the other major mitotic phosphatases PP1 and PP2A play in counteracting Aurora A. PP1 and PP2A inhibition with calyculin A caused a complete upshift of NDC80 on Phos-tag gels and a large increase in NDC80 pS55 in both parental and PPP6C KO cells (Fig. 5A). This upshift and NDC80 pS55 were protected from Aurora A inhibition (Fig. 5A). Both the number and intensity of NDC80 pS55 positive kinetochores increased following PP1/PP2A inhibition and this was anti-correlated with the localization of astrin (Fig. 5B-5E). Interestingly, astrin recruitment to microtubule-attached kinetochores was limited within a narrow window of NDC80 phosphorylation set by the level of PP6-regulated Aurora A activity and PP1/PP2A. Based on these observations we conclude that NDC80 does not appear to undergo full stoichiometric phosphorylation at all Aurora sites under normal conditions. Together, these observations show that NDC80 phosphorylation is dynamically modulated at microtubule-attached kinetochores rather than at checkpoint-active kinetochores or unaligned chromosomes (Fig. 2G). Furthermore, they indicate that NDC80 phosphorylation although dependent on PP6-regulated Aurora A activity, is also actively limited by counteracting PPP family phosphatases that are discrete from PP6, most likely PP1 and PP2A. This left open the question of what process the PP6-regulated pool of Aurora A is needed for and how loss of this control by PP6 leads to the formation micronuclei and abnormal nuclear structures.

Mitotic spindle size is increased in PPP6C knockout cells

Previous work has suggested that the Aurora A-TPX2 complex regulates spindle length and may thus play a role in spindle size control (Bird and Hyman, 2008). We therefore predicted that removal of PP6 activity should result in larger mitotic spindles. In agreement with that proposal, a significant increase in mean metaphase spindle size from 9 to 12 µm was observed in PPP6C KO cells, without any major increases in chromosome numbers (Fig. 6A to 6C). In fact, for PPP6C KO cells, more broken chromosomal fragments were seen and flow cytometry indicated progressive loss rather than gain of chromosomes (Fig. 6B and 6C), changes unlikely to explain increased spindle size. This is in agreement with our previous characterization of cells lacking PPP6C, which showed a pattern of single chromosome mis-segregation events rather than large changes to ploidy (Hammond et al., 2013). Fitting with the known relationship between Aurora

A and PP6 (Zeng et al., 2010), inhibition of Aurora A resulted in smaller spindles in both parental and PPP6C KO cells (Fig. 6D). Supporting the view this is a general consequence of PP6 inactivation, the increase in spindle size was also observed in the PPP6C KO eHAP haploid cell lines used for functional genomics (Fig. S1). Removal of PP6 thus uncouples spindle size control from chromosome number, most likely through its role in the regulation of Aurora A activity.

To test if increased spindle size was caused by increased spindle pole separation or by other process altering the balance of forces within the spindle, monopolar spindle assays were used. Similar to the effects on metaphase spindles, monopolar spindles were larger in PPP6C KO cells, whereas Aurora A inhibition reduced the size of monopolar spindles in both parental and PPP6C KO cells (Fig. 6E). In contrast, Aurora B inhibition resulted in larger monoastral spindles with more dispersed chromosomes (Fig. 6E), supporting the view it has different functions to Aurora A. Thus, the larger spindle size observed in PPP6C KO cells is Aurora A activity dependent, but does not appear to be explained by altered regulation of spindle pole separation since monoastral spindle size was also increased. Interestingly, astrin, underwent Aurora A-sensitive redistribution from kinetochores to spindle poles in metaphase and anaphase in PPP6C KO cells (Fig. 6F and 6G). This effect was specific to astrin, since core centromere and kinetochore proteins CENP-A and NDC80 were not altered at metaphase, anaphase, or monoastral spindles (Fig. S8). However, since the astrin-kinastrin complex interacts with NDC80 and contributes to microtubule attachment stability (Dunsch et al., 2011; Kern et al., 2017), altered regulation of kinetochores by Aurora A in PPP6C KO cells could explain the effects on spindle size. These changes had notable functional consequence. The enlarged spindles in PPP6C KO cells showed less compact metaphase plates and failed to tightly hold segregating chromosomes into compact units in anaphase, resulting in the formation of aberrant nuclei and micronuclei (Fig. 7A) (Hammond et al., 2013). These enlarged spindles also took significantly longer to align chromosomes to the metaphase plate and enter anaphase (Fig. 7B) (Zeng et al., 2010),

NDC80 phosphorylation regulates mitotic spindle size and chromosome segregation

We therefore asked if altered NDC80 phosphorylation can explain the difference in spindle size control and chromosome segregation leading to micronucleation and nuclear morphology defects in PPP6C KO cells. For this purpose, cell lines conditionally expressing either GFP-tagged wild type NDC80, phosphorylation deficient (NDC80-9A), or phospho-mimetic (NDC80-9D) variants in which nine Aurora kinase consensus sites had been mutated were used (Fig. S9A) (Guimaraes et al., 2008). In a parental background with wild-type PPP6C, expression of NDC80-9A or NDC80-9D resulted in smaller or larger metaphase spindles, respectively, compared the wild type NDC80 protein (Fig. 8A and 8B). Similarly, monoastral spindles were smaller or larger in parental cells expressing NDC80-9A or NDC80-9D (Fig. 8C and 8D), respectively. Supporting the view that NDC80 is a key target for Aurora A, spindle size was the same in NDC80-9A and NDC80 WT cells treated with Aurora A inhibitor (Fig. S9B and S9C). Furthermore, NDC80-9A was dominant over PPP6C depletion for spindle size (Fig. 8C and 8D) and rescued astrin localization to kinetochores (Fig. 8C and 8E). This supports the conclusion that the elevated NDC80 phosphorylation in PPP6C-depleted cells is responsible for both increased spindle size and astrin loss from kinetochores. Together, these observations show that NDC80 is a key target of Aurora A, and explain the enlarged spindle size and consequent chromosome mis-segregation in cells lacking PP6 activity. To further test this idea, we asked if NDC80-9A can suppress nuclear morphology defects in cells lacking PP6. When compared to expression of the wild-type

protein, NDC80-9A suppressed the frequency of nuclear shape defects in PPP6C depleted cells (Fig. 8F and 8G). In contrast, NDC80-9D strongly exacerbated the nuclear shape defects (Fig. 8F and 8G). This latter observation is in agreement with the observation that PPP6C KO results in a partial increase in NDC80 phosphorylation, but does not create the fully stoichiometrically phosphorylated state equivalent to NDC80-9D seen with PP1/PP2A inhibition.

PPP6C knockout cells are dependent on the spindle checkpoint for survival

Our results suggest that Aurora A and Aurora B have opposing activities in mitosis, rather than showing convergent regulation of NDC80 in spindle formation, error correction and checkpoint signaling. Aurora A is not required for spindle checkpoint signaling, but removal of PPP6C delays mitotic progression suggesting a prolonged period of checkpoint activation. To test this idea, we asked if PPP6C KO cells with increased Aurora A activity become more dependent on the spindle assembly checkpoint. Cells lacking PPP6C become highly sensitive to inhibitors of the spindle checkpoint kinase MPS1 and show further increased nuclear morphology defects (Fig. 8H and 8I), and a significant reduction in cell survival compared to isogenic parental cells (Fig. 8J and Fig. S10A-S10C). In parental cells, Aurora A and MPS1 inhibition synergize, whereas in PPP6C KO cells with amplified Aurora A activity this combination was less effective than MPS1 inhibition alone (Fig. 8I-8J). This slightly reduced effect may be due to the increased level of active Aurora A in PPP6C KO cells compared to the parental control cells, resulting in residual active kinase at the spindle when the Aurora A inhibitor is present (Fig. 6D). Importantly, NDC80 phosphorylation was not reduced even when the MPS1-inhibitor was used at high doses (Fig. S10D), showing MPS1 is not the major kinase for the NDC80 phosphorylation events studied here.

Discussion

Mitotic spindle size control and genome instability

How mitotic spindle size is controlled to ensure accurate chromosome segregation, and the way this control is modified in aneuploid tumor cells are important questions for cell biology. Although it is widely accepted that the mitotic spindle scales with the number of chromosomes, the existence of such a scaling mechanism is counterintuitive since it would seem to benefit aneuploid tumor cells with increased numbers of chromosomes, rather than normal diploid cells which don’t typically regulate their ploidy. If spindle size was fixed, then highly aneuploid or tetraploid cells would be eliminated upon cell division. Spindle size control must therefore serve another purpose in somatic cells. NDC80 is the keystone protein for spindle formation, and when removed or inactivated mitosis fails catastrophically (Chen et al., 1997; McCleland et al., 2003). This is due to its role in integration of chromosome attachment to microtubules and chromosome alignment with checkpoint signaling, and as we show here spindle size control. By studying specific point mutants, we find NDC80 is a key regulatory target for the PP6-regulated pool of Aurora A. Rather than being a switch-like mechanism to control microtubule binding as proposed for Aurora B (Cheeseman et al., 2006; Ciferri et al., 2008), we propose that this Aurora A-dependent regulation serves to minimize the spindle and ensure a highly compacted metaphase plate and maintenance of a compressed body of segregating chromosomes in anaphase. This tight compaction is important for the formation of a single nucleus in G1, and accordingly removal of PPP6C results in micronucleation and other structural defects in the nuclei. Intriguingly, removal

of PPP6C causes micronucleation in both haploid and highly aneuploid cell lines, suggesting that this is a direct effect of PPP6C removal and not an indirect effect of changes in ploidy.

Aurora A and Aurora B function at the kinetochore – a relationship under tension

Current thinking has largely ascribed NDC80 phosphorylation to Aurora B-mediated error correction and spindle checkpoint signaling in the absence of tension (Lampson and Cheeseman, 2011; Liu et al., 2009; Musacchio, 2015). Contrary to these ideas, we find that Aurora A is the major kinase phosphorylating NDC80 at microtubule-attached kinetochores during spindle formation. Both the temporal distribution from prometaphase into anaphase, and association with microtubule-attached, rather than checkpoint active, kinetochores argue against functions in Aurora B-mediated error correction and spindle checkpoint signaling. Furthermore, we demonstrate that phospho-regulation of NDC80 at microtubule-attached kinetochores by the PP6 regulated pool of Aurora A is necessary to control metaphase spindle size rather than initiate checkpoint signaling. Previous work found that TPX2 mutants unable to bind Aurora A formed short spindles capable of chromosome segregation (Bird and Hyman, 2008). This is similar to the behavior of cells expressing NDC80-9A Aurora-phosphorylation deficient mutants. Further work will be needed to explain precisely how NDC80 phosphorylation modulates its function and the behavior of astrin, but clues are already provided in published work showing that Aurora phosphorylation of NDC80 modulates its interaction with microtubules and balance of forces within the spindle, promoting oscillatory chromosome movements linked to Aurora A activity (DeLuca et al., 2018; Iemura et al., 2021; Long et al., 2017; Umbreit et al., 2012). The observations that PPP6C-depletion or knockout results in altered astrin localization, and this is rescued by NDC80-9A mutants also support the view that Aurora A phosphorylation controls the properties of the kinetochore. Although astrin is not essential for microtubule binding to kinetochores, it slows movement on the kinetochore on microtubules and stabilizes correctly bioriented attachments (Rosas-Salvans et al., 2022). Thus, we propose that PP6 limits Aurora A activity at microtubule-attached kinetochores to fine tune their properties during spindle scaling, and this regulation ensures that chromosome segregation leads to the formation of equal nuclei lacking structural defects. This is conceptually different to current ideas that have focused on explaining roles for Aurora A and Aurora B phosphorylation of NDC80 in different forms of error correction and spindle checkpoint signaling.

Other recent evidence also shows there is a need to revise our views on the mechanisms of error correction and spindle checkpoint signaling. New work shows that MPS1 is initially recruited to microtubule-attached kinetochores and actively promotes microtubule release and checkpoint activation (Hayward et al., 2022). Aurora B activity but not NDC80 phosphorylation was necessary for MPS1-recruitment and spindle checkpoint signaling (Hayward et al., 2022; Nijenhuis et al., 2013). This relationship remains in force even in PPP6C KO cells with amplified Aurora A activity, which as we show here still depend on Aurora B but not Aurora A for checkpoint signaling. How do we explain some of the differences between our observations and other studies? Previous work has largely relied on the use of NDC80 phospho-mimetic and phospho-null mutants, often without validation that these phospho-sites are actually Aurora B sites in vivo under the specific conditions being used. Additionally, common Aurora B inhibitors are not completely specific to Aurora B and also inhibit Aurora A (de Groot et al., 2015). It is therefore important that inhibitors to both kinases are carefully titrated and tested in parallel as we have done here. In some studies, FRET sensors for Aurora B have been used in to show that its activity at the centromere is sensitive to microtubule attachment at kinetochores and

correlated with the effects of expressing mutant NDC80 proteins (Yoo et al., 2018). However, this does not prove NDC80 is the crucial target for Aurora B, and with such approaches it is important to directly confirm when and where NDC80 is phosphorylated as we have done with biochemical and microscopy-based approaches. We also find that Aurora B inhibition leads to more scattered chromosomes in monopolar spindle assays, whereas both Aurora A inhibition and expression of NDC80-9A result in compact monopoles. We therefore suggest that the effects of Aurora B inhibition are largely indirect through its role in MPS1 recruitment, which appears to be the major kinase activity disrupting kinetochore-microtubule attachments possibly via NDC80 phosphorylation at other sites or phosphorylation of the Ska complex (Hayward et al., 2022; Maciejowski et al., 2017; Sarangapani et al., 2021).

To explain these findings, we conclude there must be other crucial targets for Aurora B that cannot be accessed by Aurora A shedding doubt on the view that tension-dependent phosphorylation and dephosphorylation of NDC80 by Aurora-kinases directly control error correction and spindle checkpoint signaling in human cells. Aurora B also phosphorylates and regulates components important for assembly of the microtubule-binding components of the kinetochore with the inner centromere (Petrovic et al., 2016). An important conclusion of our work is therefore that Aurora A and Aurora B must play specific roles at the outer kinetochore and inner centromere, respectively. Exploring how microtubule-binding and the generation of force regulate Aurora B activity and phosphorylation at the inner centromere is therefore an important question for future work in this area.

Altered Aurora A regulation creates spindle checkpoint dependency

In addition to shedding light on the cellular functions of Aurora A, PP6 and NDC80, these findings have relevance for cancer biology. Aurora A amplification or inactivation of PPP6C through mutation are seen in a number of cancers and have been associated with, and are considered drivers for, aneuploidy (Anand et al., 2003; Bischoff et al., 1998; Hammond et al., 2013; Hodis et al., 2012; Krauthammer et al., 2012; Sen et al., 1997). As we show here, Aurora A and PP6 are important to control spindle size and thus support high fidelity chromosome segregation. However, any benefit must come at a cost, since PPP6C KO cells show delayed progression through mitosis, and are more dependent on the spindle checkpoint. MPS1 inhibition thus targets cells with elevated Aurora A activity due to loss of PPP6C, supporting the view this is an effective way to selectively eliminate some aneuploid cancer cells (Cohen-Sharir et al., 2021). However, as our work shows aneuploidy may not be the sole determinant for this sensitivity. In our experiments, we compare highly aneuploid parental and PPP6C KO cell lines, and find only the latter are sensitive to a spindle checkpoint inhibitor. Although amplified for Aurora A activity, an Aurora A inhibitor had little effect on the viability of PPP6C KO cells, and in fact partially suppressed cell death induced by MPS1 inhibition. This may explain the lack of success of Aurora A inhibitors in clinical trials. Further work is needed to develop these ideas and target the key dependencies created by oncogenic mutations in PPP6C driving genome instability, and as we show here MPS1 is candidate worthy of attention. However, this will need to take into account specific genetic changes driving genome instability, as well as alterations to ploidy, if it is to succeed in first generating and then applying new anti-cancer therapies.

Acknowledgments

We thank our colleagues in the Barr and Gruneberg groups for much helpful discussion and support. This work was supported by a Cancer Research UK program grant award C20079/A15940 (FAB, TS, KK, SS, LJF) and UK Medical Research Council Senior Non-Clinical Research fellowship MR/K006703/1 (UG, DH).

Author contributions

Conceptualization: FAB; Methodology: SS, TS, KMK, ER, FAB; Investigation: TS, KMK, SS, CB, SK, CN, DH, LJF; Funding acquisition: FAB, UG; Supervision: FAB, UG; Writing – original draft: FAB; Writing – review and editing: FAB, TS, KMK, LJF, UG.

Competing interests

Authors declare that they have no competing interests.

Materials and Methods

Reagents and antibodies

General laboratory chemicals were obtained from Merck and Thermo Fisher Scientific. Commercially available polyclonal antibodies (pAbs) or monoclonal antibodies (mAbs) were used for pT288 Aurora A (rabbit mAb; Cell Signalling Technology, 3079S), Aurora A (rabbit mAb; Cell Signalling Technology, 4718S), pan Aurora (Phospho-Aurora A (Thr288)/Aurora B (Thr232)/Aurora C (Thr198); rabbit mAb, Cell Signalling Technology, 2914S), Aurora B (mouse mAb, BD Transduction labs, 611083), pT232 Aurora B (rabbit pAb, Rockland, 600-401-677), PPP6C (rabbit, mAb, AbCam, ab131335), NDC80 pS55 (rabbit pAb, GeneTex, GTX70017), NDC80 (for immunoprecipitation and immunoblotting: mouse mAb, Santa Cruz, sc-515550; for immunoprecipitation only: rabbit pAb, ProteinTech, 18932-1-AP and mouse mAb, AbCam, ab3613, for immunofluorescence: mouse mAb, AbCam, ab3613), MPS1 (rabbit pAb, ProteinTech, 10381-1-AP), Cyclin B1 (mouse mAb; Millipore, 05-373), pT320 PPP1CA (rabbit mAb, AbCam, ab62334), PPP1CA (rabbit pAb, Bethyl Laboratories, A300-904A), pT481 PRC1 (rabbit mAb, AbCam, ab62366), tubulin (mouse mAb; Merck, T6199), BUB1 (rabbit pAb, Bethyl Laboratories, A300-373A), BUBR1 (mouse mAb, Merck, MAB3612), CENP-A (mouse mAb, AbCam, ab13939; mouse mAb, GeneTex, GTX13939), CENP-C (guinea pig pAb, MBL life science, PD030), CREST (human pAb, Antibodies Inc., 15-234), Mab414 (mouse mAb, AbCam, ab24609), NUP153 (rabbit pAb, Bethyl Laboratories, A301-788A), TPX2 (mouse mAb, AbCam, ab32795), Mad1 (rabbit pAb, GeneTex, GTX105079). Antibodies against Aurora A (for immunofluorescence: sheep pAb), Astrin (rabbit, pAb), Kinastrin, (sheep, pAb), mCherry (sheep, pAb) and GFP (sheep, pAb) were described previously (Bastos and Barr, 2010; Dunsch et al., 2011; Thein et al., 2007; Zeng et al., 2010).

NDC80 phospho-antibodies were raised to Aurora-sites described in the literature (Kettenbach et al., 2011). Custom rabbit pAb anti-pS62 and anti-pT61-pS62 NDC8080 were raised by Eurogentec using a 28-day protocol. For immunisations, peptides CLFGKRT-S(PO_3H_2)-GHGSRN and CSLFGKR-T(PO_3H_2)-S(PO_3H_2)-GHGSRN fused to KLH carrier protein were used respectively. Total IgG were isolated from post-immune sera by affinity purification on Sepharose-protein G (Merck, Cytiva 17-0618-05). Custom sheep pAb anti-pS55 NDC80 pAb

was raised by the Scottish Blood Transfusion Service using a 4-month long program. For immunisations, peptide CSERKVS(PO_3H_2)LFGKR was fused to KLH carrier protein. Total IgG were isolated from post-immune sera by affinity purification on Sepharose-protein G. NDC80 pS55 specific antibodies were further immuno-purified by incubation with the phosphopeptide antigen immobilized on Sulfo-Link Coupling Gel (Pierce, 20401). Secondary donkey antibodies against mouse, rabbit or sheep, labelled with HRP were purchased from Jackson ImmunoResearch Laboratories (715-035-150, 711-035-152, 713-035-147 respectively). Secondary antibodies for immunofluorescence were purchased from ThermoFisher Scientific and Jackson ImmunoResearch Laboratories.

Expression plasmid and CRISPR gRNA construction

CRISPR-Cas9 plasmids were as follows: pSpCas9(BB)-2A-Puro (PX459) V2.0 (Addgene 62988; a gift from Feng Zhang; Ran et al., 2013) was digested with BbsI, and the guide RNA sequence targeting human PPP6C (5'- GCTAGACCTGGACAAGTATG-3') was inserted by annealed oligonucleotide cloning. LentiCRISPR v2-Blast (Addgene 83480; a gift from Mohan Babu) and lentiCRISPR v2 (Addgene 52961; a gift from Feng Zhang; Sanjana et al., 2014) were digested with BsmBI, and the guide RNA sequences targeting human PPP6C (5'-ACAGTGTGTGGAGATATCCA-3') and human NDC80 (guide #1, 5'-CTCACGTTTGAGGGGTATAG-3'; guide #2, 5'-GTGTATTCGACAACTCTGTG-3'; guide #3, 5'-CTGGGATCTTAACTCCTGCA-3'), respectively, was inserted by annealed oligonucleotide cloning.

Human NDC80 was amplified from human testis cDNA (Marathon cDNA, Takara Bio Inc.) using Pfu polymerase (Promega). Mammalian expression constructs were based on pcDNA5/FRT/TO vectors, modified to encode the NDC80-GFP reading frames. To generate phospho-null (9A) or phospho-mimetic (9D) NDC80 phosphorylation sites, the site encoding amino acids Ser4, Ser5, Ser8, Ser15, Ser44 Thr49, Ser55, Ser62 and Ser69 were changed to either alanine (9A) or aspartic acid (9D) by mutagenesis.

Cell lines and cell culture

HeLa, HEK293T and HEK293FT cell lines were purchased from ATCC and cultured in DMEM, high glucose, GlutaMAX™ Supplement, pyruvate (#10569010, Gibco™, Thermo Fisher Scientific) supplied with 10% fetal bovine serum (FBS, Merck). eHAP cells were purchased from Horizon Discovery (C669) and cultured in IMDM (#12440061, Gibco™, Thermo Fisher Scientific) supplied with 10% FBS. All cells were cultured at 37°C and 5% CO_2. CRISPR/Cas9-edited HeLa cells with an inserted GFP tag in the C-terminus of MPS1 gene (HeLa MPS1-GFP^{CRISPR}) have been described previously (Alfonso-Pérez et al., 2019).

To generate eHAP PPP6C KO cells, parental haploid eHAP cells were transfected with pSpCas9(BB)-2A-Puro (PX459) V2.0 containing the guide RNA sequence targeting human PPP6C. Non-transfected cells were killed with transient 2-day puromycin selection and then cell colonies expanded in non-selective medium to be analysed by immunoblotting and sequencing. To generate HeLa PPP6C KO cells, lentiCRISPR v2-Blast containing the guide RNA sequence targeting human PPP6C, pMD2.G and psPAX2 (Addgene 12259 and 12260, respectively; gifts from Didier Trono) were used for lentiviral-based packaging from HEK293T cells, and the supernatant was used to infect HeLa cells. After infection, antibiotic-resistant clones were selected by blasticidin and expanded in non-selective medium to be analysed by immunoblotting. HeLa cell lines with single integrated copies of the desired NDC80-GFP transgene in pcDNA5/FRT/TO were created using the doxycycline-inducible T-REx Flp-In system

(Invitrogen). Transgene expression was induced by addition of 1µg/ml doxycycline (Merck, D9891) to the culture medium for minimum of 24 h.

Metaphase chromosome spreads

For chromosome spreads, 3 × 10 cm dishes per condition of 50% confluent HeLa cells were treated with 100 ng/ml nocodazole for 6 h. Following treatment, mitotic cells were isolated by shake-off, and pelleted at 300 × g for 4 min at 37°C in a 15 ml Falcon tube. Cells were resuspended in 5 ml KCl (75 mM), which had been pre-warmed to 37°C. Cells were incubated at 37°C for 30 min, with gentle inversion of the tube every 5 min to help prevent cell clumping. Cells were pelleted at 300 × g for 4 min at 37°C, and the KCl solution was decanted. Cells were resuspended in the residual volume of KCl that remained in the tube. Cells were fixed in 1 mL cold fixative (3:1 ratio of MeOH and glacial acetic acid), whilst gently vortexing the cells. An additional 9 ml cold fixative was added to the tube, and fixed cells stored in the fridge at 4°C overnight. The next day, fixed cells were pelleted at 300 × g for 4 min at room temperature and the fixative decanted. Cells were resuspended in 1 ml cold fixative. Sterile glass microscopy slides were washed in distilled/deionised water, and placed at 45° angles against a tube rack. A 100 µl aliquot of fixed cells was then dropped onto the slides from a height of around 50 cm. Slides were then washed by gently applying cold fixative over the slides with a Pasteur pipette. The slides were then placed on a wet paper towel above a heat block set to 80°C for 2 min to dry. Slides were allowed to dry at room temperature before application of Mowiol mounting medium containing Hoechst DNA dye (1:3000 dilution). A sterile coverslip was placed on top of the Mowiol drops and slides were placed in the fridge at 4°C overnight to dry. Slides were imaged using a 100X oil objective, on an Olympus BX61 fixed cell microscope.

Flow cytometry profiling of DNA content and cell cycle stage

HeLa cells grown in culture were trypsinized and pelleted at 500 × g for 3 min at 37°C in a 15 mL Falcon tube. The media was decanted and cells were gently resuspended in 1 ml PBS. Cells were pelleted at 500 × g for 3 min at 37°C, and the supernatant decanted. Cells were resuspended in 90% (vol/vol) ice-cold MeOH in distilled/deionised water, whilst gently vortexing to help prevent cell clumping. Cells were fixed at -20°C overnight. The next day, fixed cells were adjusted to 5×10^5 cells/mL and pelleted at 500 × g for 3 min at room temperature. Cells were resuspended in 300 µl staining buffer (50 µg/mL propidium iodide (P4864, Sigma-Aldrich) and 50 µg/ml RNase (Roche, 11119915001)) in PBS. Stained cells were incubated at room temperature for 1 h, protected from light. Samples were then analysed and data acquired using a BD LSRFortessa X20 flow cytometer. Data was visualised using FlowJo 10.8.1 (TreeStar, BD).

Genome-wide CRISPR knockout screen for synthetic growth defects with PPP6C

Human genome targeting CRISPR Knock-Out (GeCKO) v2 lentiviral pooled libraries (A and B libraries) were purchased from Addgene and amplified according to a published protocol (Sanjana et al., 2014). A genome-wide CRISPR screen was performed as described previously (Joung et al., 2017). Briefly, lentivirus produced by HEK293FT cells was tested to achieve an MOI of 0.3 in eHAP parental and PPP6C KO cells. A total of 2×10^8 cells were transduced with GeCKO v2 libraries A and B. After 24 h, the cells were treated with 1.5 µg/ml puromycin, which was replaced with non-selective medium five days later. A minimum of 1.2×10^8 cells were maintained throughout the screen. Subsequently, 1×10^7 cells were used for genomic DNA extraction. Library preparation for Next Generation Sequencing (NGS) by PCR amplification of sgRNA inserts from 108 µg of parental or PPP6C KO cell genomic DNA using NEBNext® Ultra™ II Q5® Master Mix (M0544L). The PCR products were purified and sequenced on

Illumina NextSeq with 80 cycles of read 1 (forward) and 8 cycles of index 1 in the Next Generation facility at the Wellcome Trust Centre of Human Genetics, University of Oxford. Quality control, normalisation, and identification of positively and negatively selected genes was performed using the Model based Analysis of Genome-wide CRISPR-Cas9 pipeline (MAGeCKFlute) (Wang et al., 2019), and the summary output is provided in Table S1. Further data analysis and graph plotting was performed in Microsoft Excel.

Clonogenic survival assays

Cells were seeded in 6-well plates (500-2,000 HeLa or 5,000-12,000 eHAP cells per well) and treated with indicated concentration of MPS1-i or AurA-i, or transduced with lentivirus derived from lentiCRISPR v2, which expressed sgRNAs targeting human NDC80. Puromycin-containing medium (1 µg/ml) was added 3 days after the lentiviral transduction. Medium containing the inhibitors or puromycin was refreshed every 2-3 days. After 7-11 days, colonies were fixed with 4% (w/v) PFA in PBS and stained with 5% (w/v) crystal violet in 25% (v/v) methanol for 10 min. The staining solution was aspirated, and the plates were rinsed by water, before air-drying at room temperature. After the plates were photographed, the retained dye was solubilised with 100% methanol to measure absorbance at 540 nm.

Gene silencing (RNAi) and RNAi rescue assays

RNA duplexes were purchased from Dharmacon and Qiagen (listed in Table S2). Cells were transfected with siRNA using Oligofectamine for the times described in the figure legends. For RNAi rescue assays, NDC80-GFP transgenes were induced by 1 µg/ml doxycycline, while endogenous NDC80 was depleted using oligonucleotides against the 5' -UTR (5'-CCCUGGGUCGUGUCAGGAA[dTdT]-3').

End point analysis of NDC80 phosphorylation and dephosphorylation

HeLa cells were arrested in mitosis using either 100 ng/ml nocodazole (Merck, 487928) or 10 µM STLC (Merck, 164739-5G) for 2.5 hrs (immunofluorescence) or 18 hrs (immunoblotting). For biochemical analysis, mitotic cells were harvested by shake-off, washed twice in PBS, and once in Opti-MEM, both of which had been pre-equilibrated to 37°C, 5% CO_2. Cells were counted and resuspended in pre-equilibrated Opti-MEM to give 7.5×10^6 cells/ml. Subsequently cells were either treated with 0.5 µM Aurora A inhibitor MLN8237 (ApexBio, A4110-APE-10mM), 10 µM Aurora B inhibitor ZM 447439 (ApexBio, A4113-APE-10mM), 10 µM Aurora B inhibitor AZD1152 (ApexBio, A4112-APE-10mM), 25-100nM PP1/PP2A inhibitor calyculin A (TOCRIS, 1336/100U), 5-20 µM PP1 inhibitor tautomycetin (TOCRIS, 2305/50U), 40 µM proteasome inhibitor MG-132 (Merck, 474790-5MG) along with 1-10 µM MPS1 inhibitor (TOCRIS, AZ3146) or DMSO (Merck, D8418) for up to 25min.

For immunofluorescence microscopy, nocodazole- or STLC-arrested cells were treated with 20 µM MG132 for 30 min and the inhibitors described above prior to fixation. Asynchronous cultures were treated with MG132 for 2.5 hrs, or 300nM CENP-E inhibitor (TOCRIS, GSK923295) for 3 hrs and 20 µM MG-132 for 30 min before fixation.

Mitotic exit time courses for NDC80 phosphorylation state

For analysis of mitotic exit time, HeLa cells were arrested with nocodazole, collected by shake-off released into nocodazole-free Opti-MEM at 37°C, 5% CO_2 for 25 min to allow mitotic spindle formation. After 25 min, cell suspensions were treated with 20 µM CDK inhibitor flavopiridol (TOCRIS, 3094/10) for up to 40 min. At each time point cells were harvested for NDC80 immunoprecipitations or western blot analysis.

NDC80 immunoprecipitations and western blot analysis

Pellets of 2.25 × 10^6 cells were lysed in 0.6 ml of lysis buffer (50 mM HEPES pH 8, 100 mM KCl, 50mM EDTA, 1% IGEPAL, 0.25% Triton X-100, 1 mM DTT, 1mM PMSF (ThermoFisher Scientific, 36978), 1:250 Protease Inhibitor Cocktail (Merck, P8340-5ML), 1:100 Phosphatase Inhibitor cocktail 3 (Merck, P0044-5ML), 100 nM okadaic acid (Enzo LifeSciences, ALX-350-011-M001) 50 U micrococcal nuclease (New England Biolabs, M0247S)). Cells lysates were either mixed with 3 × Laemmli buffer for immunoblotting analysis or subject to pre-clearing and NDC80 complexes were isolated by 2-h incubation at 4°C with anti-NDC80 antibody cocktail (ProteinTech, 18932-1-AP; Abcam, ab3613; SantaCruz, sc-515550) and 20 µl protein G–Sepharose (Merck, GE17-0618-01). The sepharose beads were washed twice with lysis buffer, once with PBS and resuspended in 1 × Laemmli buffer. To control for antibody specificity, PBS-washed Ndc80 immuno-precipitates were subject to two further washes in λ-phosphatase buffer, treated with 400 U of λ-phosphatase (New England Biolabs, P0753L) for 45 min at room temperature and then mixed with 3 × Laemmli buffer. For immunoblotting, proteins were separated by SDS-PAGE and transferred onto nitrocellulose membrane using a Trans-blot Turbo system (Bio-Rad, 1704159). All Western blots were revealed using ECL (GE Healthcare, RPN2106 and GE Healthcare, GE28-9068-37). Protein concentrations were measured by Bradford assay using Protein Assay Dye Reagent Concentrate (Bio-Rad, 5000006).

NDC80 and dephosphorylation time course assays

Nocodazole-arrested HeLa cells were harvested by shake-off, washed twice in ice-cold PBS, lysed on ice at 1 × 10^6 cells/ml ice-cold lysis buffer either deprived of phosphatase inhibitors or containing 100 nM okadaic acid. At the indicated timepoints okadaic acid was supplemented to a final concentration of 1.6 µM and lysates were mixed with 3 × Laemmli buffer for immunoblotting.

Phos-tag gel analysis of NDC80 phosphorylation state

To reveal differently phosphorylated forms of NDC80, cell lysates were precipitated on magnetic carboxylate modified beads (Merck, GE45152105050250) in the presence of 77% (volv/vol) acetonitrile (Merck, 271004) for 30min at room temperature, washed twice with 70% (vol/vol) ethanol and resuspended in 1 × Laemmli buffer supplemented with 100 µM $MnCl_2$ (Hughes et al., 2014; Hughes et al., 2019). We found this approach removes components of the lysis buffer and cell lysates that interfere with the resolution of phosphorylated proteins in the next step. Subsequently, samples were resolved on a gel supplemented with 25 µM Phos-tag (Alpha Laboratories Ltd) and 100 µM $MnCl_2$ (Kinoshita et al., 2006). Prior to protein transfer onto the nitrocellulose membrane, gels were soaked for 30min in SDS-PAGE running buffer supplemented with 10 mM EDTA.

Immunofluorescence microscopy of mitotic spindles

Cells plated on glass coverslips were fixed and permeabilised with ice-cold methanol for 5 min on ice, or with 3% (wt/vol) PFA in PBS at room temperature for 15-20 min, followed by permeabilization with 0.2% (vol/vol) Triton X-100 in PBS at room temperature for 5-10 min. Combined PTEMF (20 mM Pipes-KOH, pH 6.8, 0.2% (vol/vol) Triton X-100, 1 mM $MgCl_2$, 10 mM EGTA, and 4% (vol/vol) formaldehyde) fixation and permeabilization for 12 min was used for detection of NDC80 pS55 and pS62, BUB1, BUBR1, CENP-A and CENP-C. Antibody dilutions were performed in PBS. Samples were imaged on a standard upright microscope system (BX61, Olympus) with filter sets for DAPI, GFP/Alexa Fluor 488, Cy3/Alexa Fluor 555

and Cy5/Alexa Fluor 647 (Chroma Technology Corp.), a 2048 × 2048-pixel complementary metal oxide semiconductor camera (PrimΣ, Photometrics), and MetaMorph 7.5 imaging software (Molecular Devices). Illumination was provided by an LED light source (pE300, CoolLED Illumination Systems). Image stacks with a spacing of 0.4 µm through the cell volume were maximum intensity projected and cropped in Image J (National Institutes of Health). For high-resolution imaging, cells were imaged under an FV3000 confocal microscope using FV31S-SW software (Olympus; 60× 1.40 NA oil-immersion objective; Galvano scanner type, 10 µsec/px scan speed, 1024 × 1024 px scan size, 2× zoom, 0.42 µm step size), and the images were processed in Image J.

Time lapse imaging of chromosome alignment and segregation in mitosis

Cells were plated in 35-mm dishes with a 14-mm 1.5 thickness coverglass window on the bottom (MatTek Corp. SiR-DNA (Spirochrome) was added at a concentration of 50 nM 2-3 hours before imaging. For imaging, the dishes or plates were placed in a 37ºC and 5% CO_2 environment chamber (Tokai Hit) on the microscope stage. Imaging was performed on an Ultraview Vox spinning disk confocal system running Volocity 6 (PerkinElmer) using a standard inverted microscope (IX81, Olympus) equipped with an electron multiplying charge coupled device camera (C9100-13, Hamamatsu Photonics). Image stacks with 15 planes and 0.6-µm apart were maximum intensity projected and cropped in Image J (National Institutes of Health).

Measurement of mitotic spindle size and kinetochore intensities

All image processing and analysis was performed using ImageJ. To measure bipolar or monoastral spindle size, a circle was drawn around the spindle capturing the spindle poles and chromosomes. The diameter of this circle was taken as spindle length. Kinetochore intensities for each fluorescent channel were determined by placing 5-to-8-pixel-diameter circular region of interests (ROIs) at the maxima of individual kinetochores, and the mean pixel intensity of each kinetochore ROI was measured and subtracted from a mean background.

Statistical analysis

Statistical analysis was performed using GraphPad Prism 9.3.1 (GraphPad Software). Statistical significance was analysed using an unpaired two-tailed t-test with Welch's correction, a one-way ANOVA, a Brown-Forsythe ANOVA, a Kruskal-Wallis test, or Dunn's multiple comparison test. Graphs display the SEM or mean ± SD as indicated in the figure legends. P-values shown on graphs are as follows: $p \geq 0.05$ = not significant (n.s.), $p < 0.05$ = *, $p < 0.01$ = **, $p < 0.001$ = ***, $p < 0.0001$ = ****.

To estimate the effect sizes for kinetochore intensities in Figure S14, pooled data was analysed in R using the open-source package dabestr (Ho et al., 2019). Mean differences are plotted as bootstrap sampling distributions for 5000 bootstrap samples. Each mean difference is depicted as a dot. Each 95% confidence interval is indicated by the ends of the vertical error bars; the confidence interval is bias-corrected and accelerated.

References

Anand, S., S. Penrhyn-Lowe, and A.R. Venkitaraman. 2003. AURORA-A amplification overrides the mitotic spindle assembly checkpoint, inducing resistance to Taxol. *Cancer Cell*. 3:51-62.

Bakhoum, S.F., B. Ngo, A.M. Laughney, J.A. Cavallo, C.J. Murphy, P. Ly, P. Shah, R.K. Sriram, T.B.K. Watkins, N.K. Taunk, M. Duran, C. Pauli, C. Shaw, K. Chadalavada, V.K. Rajasekhar, G. Genovese, S. Venkatesan, N.J. Birkbak, N. McGranahan, M. Lundquist, Q. LaPlant, J.H. Healey, O. Elemento, C.H. Chung, N.Y. Lee, M. Imielenski, G. Nanjangud, D. Pe'er, D.W. Cleveland, S.N. Powell, J. Lammerding, C. Swanton, and L.C. Cantley. 2018. Chromosomal instability drives metastasis through a cytosolic DNA response. *Nature*. 553:467-472.

Bastos, R.N., and F.A. Barr. 2010. Plk1 negatively regulates Cep55 recruitment to the midbody to ensure orderly abscission. *J Cell Biol*. 191:751-760.

Bayliss, R., T. Sardon, I. Vernos, and E. Conti. 2003. Structural basis of Aurora-A activation by TPX2 at the mitotic spindle. *Mol Cell*. 12:851-862.

Bird, A.W., and A.A. Hyman. 2008. Building a spindle of the correct length in human cells requires the interaction between TPX2 and Aurora A. *J Cell Biol*. 182:289-300.

Bischoff, J.R., L. Anderson, Y. Zhu, K. Mossie, L. Ng, B. Souza, B. Schryver, P. Flanagan, F. Clairvoyant, C. Ginther, C.S. Chan, M. Novotny, D.J. Slamon, and G.D. Plowman. 1998. A homologue of Drosophila aurora kinase is oncogenic and amplified in human colorectal cancers. *EMBO J*. 17:3052-3065.

Carazo-Salas, R.E., G. Guarguaglini, O.J. Gruss, A. Segref, E. Karsenti, and I.W. Mattaj. 1999. Generation of GTP-bound Ran by RCC1 is required for chromatin-induced mitotic spindle formation. *Nature*. 400:178-181.

Carmena, M., M. Wheelock, H. Funabiki, and W.C. Earnshaw. 2012. The chromosomal passenger complex (CPC): from easy rider to the godfather of mitosis. *Nat Rev Mol Cell Biol*. 13:789-803.

Cheeseman, I.M., J.S. Chappie, E.M. Wilson-Kubalek, and A. Desai. 2006. The conserved KMN network constitutes the core microtubule-binding site of the kinetochore. *Cell*. 127:983-997.

Chen, Y., D.J. Riley, P.L. Chen, and W.H. Lee. 1997. HEC, a novel nuclear protein rich in leucine heptad repeats specifically involved in mitosis. *Mol Cell Biol*. 17:6049-6056.

Ciferri, C., S. Pasqualato, E. Screpanti, G. Varetti, S. Santaguida, G. Dos Reis, A. Maiolica, J. Polka, J.G. De Luca, P. De Wulf, M. Salek, J. Rappsilber, C.A. Moores, E.D. Salmon, and A. Musacchio. 2008. Implications for kinetochore-microtubule attachment from the structure of an engineered Ndc80 complex. *Cell*. 133:427-439.

Clarke, P.R., and C. Zhang. 2008. Spatial and temporal coordination of mitosis by Ran GTPase. *Nat Rev Mol Cell Biol*. 9:464-477.

Cohen-Sharir, Y., J.M. McFarland, M. Abdusamad, C. Marquis, S.V. Bernhard, M. Kazachkova, H. Tang, M.R. Ippolito, K. Laue, J. Zerbib, H.L.H. Malaby, A. Jones, L.M. Stautmeister, I. Bockaj, R. Wardenaar, N. Lyons, A. Nagaraja, A.J. Bass, D.C.J. Spierings, F. Foijer, R. Beroukhim, S. Santaguida, T.R. Golub, J. Stumpff, Z. Storchova, and U. Ben-David. 2021. Aneuploidy renders cancer cells vulnerable to mitotic checkpoint inhibition. *Nature*. 590:486-491.

Crasta, K., N.J. Ganem, R. Dagher, A.B. Lantermann, E.V. Ivanova, Y. Pan, L. Nezi, A. Protopopov, D. Chowdhury, and D. Pellman. 2012. DNA breaks and chromosome pulverization from errors in mitosis. *Nature*. 482:53-58.

de Groot, C.O., J.E. Hsia, J.V. Anzola, A. Motamedi, M. Yoon, Y.L. Wong, D. Jenkins, H.J. Lee, M.B. Martinez, R.L. Davis, T.C. Gahman, A. Desai, and A.K. Shiau. 2015. A Cell Biologist's Field Guide to Aurora Kinase Inhibitors. *Front Oncol*. 5:285.

DeLuca, J.G., W.E. Gall, C. Ciferri, D. Cimini, A. Musacchio, and E.D. Salmon. 2006. Kinetochore microtubule dynamics and attachment stability are regulated by Hec1. *Cell*. 127:969-982.

DeLuca, K.F., S.M. Lens, and J.G. DeLuca. 2011. Temporal changes in Hec1 phosphorylation control kinetochore-microtubule attachment stability during mitosis. *J Cell Sci*. 124:622-634.

DeLuca, K.F., A. Meppelink, A.J. Broad, J.E. Mick, O.B. Peersen, S. Pektas, S.M.A. Lens, and J.G. DeLuca. 2018. Aurora A kinase phosphorylates Hec1 to regulate metaphase kinetochore-microtubule dynamics. *J Cell Biol*. 217:163-177.

Ditchfield, C., V.L. Johnson, A. Tighe, R. Ellston, C. Haworth, T. Johnson, A. Mortlock, N. Keen, and S.S. Taylor. 2003. Aurora B couples chromosome alignment with anaphase by targeting BubR1, Mad2, and Cenp-E to kinetochores. *J Cell Biol*. 161:267-280.

Dunsch, A.K., E. Linnane, F.A. Barr, and U. Gruneberg. 2011. The astrin-kinastrin/SKAP complex localizes to microtubule plus ends and facilitates chromosome alignment. *J Cell Biol*. 192:959-968.

Fu, J., M. Bian, G. Xin, Z. Deng, J. Luo, X. Guo, H. Chen, Y. Wang, Q. Jiang, and C. Zhang. 2015. TPX2 phosphorylation maintains metaphase spindle length by regulating microtubule flux. *J Cell Biol*. 210:373-383.

Goshima, G., and J.M. Scholey. 2010. Control of mitotic spindle length. *Annu Rev Cell Dev Biol*. 26:21-57.

Gruss, O.J., R.E. Carazo-Salas, C.A. Schatz, G. Guarguaglini, J. Kast, M. Wilm, N. Le Bot, I. Vernos, E. Karsenti, and I.W. Mattaj. 2001. Ran induces spindle assembly by reversing the inhibitory effect of importin alpha on TPX2 activity. *Cell*. 104:83-93.

Gruss, O.J., M. Wittmann, H. Yokoyama, R. Pepperkok, T. Kufer, H. Sillje, E. Karsenti, I.W. Mattaj, and I. Vernos. 2002. Chromosome-induced microtubule assembly mediated by TPX2 is required for spindle formation in HeLa cells. *Nat Cell Biol*. 4:871-879.

Guimaraes, G.J., Y. Dong, B.F. McEwen, and J.G. Deluca. 2008. Kinetochore-microtubule attachment relies on the disordered N-terminal tail domain of Hec1. *Curr Biol*. 18:1778-1784.

Hammond, D., K. Zeng, A. Espert, R.N. Bastos, R.D. Baron, U. Gruneberg, and F.A. Barr. 2013. Melanoma-associated mutations in protein phosphatase 6 cause chromosome instability and DNA damage owing to dysregulated Aurora-A. *J Cell Sci*. 126:3429-3440.

Hauf, S., R.W. Cole, S. LaTerra, C. Zimmer, G. Schnapp, R. Walter, A. Heckel, J. van Meel, C.L. Rieder, and J.M. Peters. 2003. The small molecule Hesperadin reveals a role for Aurora B in correcting kinetochore-microtubule attachment and in maintaining the spindle assembly checkpoint. *J Cell Biol*. 161:281-294.

Hayward, D., E. Roberts, and U. Gruneberg. 2022. MPS1 localizes to microtubule-attached kinetochores and actively promotes microtubule release. *Submitted*.

Heald, R., R. Tournebize, T. Blank, R. Sandaltzopoulos, P. Becker, A. Hyman, and E. Karsenti. 1996. Self-organization of microtubules into bipolar spindles around artificial chromosomes in Xenopus egg extracts. *Nature*. 382:420-425.

Helmke, K.J., and R. Heald. 2014. TPX2 levels modulate meiotic spindle size and architecture in Xenopus egg extracts. *J Cell Biol*. 206:385-393.

Ho, J., T. Tumkaya, S. Aryal, H. Choi, and A. Claridge-Chang. 2019. Moving beyond P values: data analysis with estimation graphics. *Nat Methods*. 16:565-566.

Hoar, K., A. Chakravarty, C. Rabino, D. Wysong, D. Bowman, N. Roy, and J.A. Ecsedy. 2007. MLN8054, a small-molecule inhibitor of Aurora A, causes spindle pole and chromosome congression defects leading to aneuploidy. *Mol Cell Biol*. 27:4513-4525.

Hodis, E., I.R. Watson, G.V. Kryukov, S.T. Arold, M. Imielinski, J.P. Theurillat, E. Nickerson, D. Auclair, L. Li, C. Place, D. Dicara, A.H. Ramos, M.S. Lawrence, K. Cibulskis, A. Sivachenko, D. Voet, G. Saksena, N. Stransky, R.C. Onofrio, W. Winckler, K. Ardlie, N. Wagle, J. Wargo, K. Chong, D.L. Morton, K. Stemke-Hale, G. Chen, M. Noble, M. Meyerson, J.E. Ladbury, M.A. Davies, J.E. Gershenwald, S.N. Wagner, D.S. Hoon, D. Schadendorf, E.S. Lander, S.B. Gabriel, G. Getz, L.A. Garraway, and L. Chin. 2012. A landscape of driver mutations in melanoma. *Cell*. 150:251-263.

Hughes, C.S., S. Foehr, D.A. Garfield, E.E. Furlong, L.M. Steinmetz, and J. Krijgsveld. 2014. Ultrasensitive proteome analysis using paramagnetic bead technology. *Mol Syst Biol*. 10:757.

Hughes, C.S., S. Moggridge, T. Muller, P.H. Sorensen, G.B. Morin, and J. Krijgsveld. 2019. Single-pot, solid-phase-enhanced sample preparation for proteomics experiments. *Nat Protoc*. 14:68-85.

Iemura, K., T. Natsume, K. Maehara, M.T. Kanemaki, and K. Tanaka. 2021. Chromosome oscillation promotes Aurora A-dependent Hec1 phosphorylation and mitotic fidelity. *J Cell Biol*. 220.

Ji, Z., H. Gao, and H. Yu. 2015. CELL DIVISION CYCLE. Kinetochore attachment sensed by competitive Mps1 and microtubule binding to Ndc80C. *Science*. 348:1260-1264.

Joung, J., S. Konermann, J.S. Gootenberg, O.O. Abudayyeh, R.J. Platt, M.D. Brigham, N.E. Sanjana, and F. Zhang. 2017. Genome-scale CRISPR-Cas9 knockout and transcriptional activation screening. *Nat Protoc*. 12:828-863.

Kalab, P., R.T. Pu, and M. Dasso. 1999. The ran GTPase regulates mitotic spindle assembly. *Curr Biol*. 9:481-484.

Kern, D.M., J.K. Monda, K.C. Su, E.M. Wilson-Kubalek, and I.M. Cheeseman. 2017. Astrin-SKAP complex reconstitution reveals its kinetochore interaction with microtubule-bound Ndc80. *Elife*. 6.

Kettenbach, A.N., D.K. Schweppe, B.K. Faherty, D. Pechenick, A.A. Pletnev, and S.A. Gerber. 2011. Quantitative phosphoproteomics identifies substrates and functional modules of Aurora and Polo-like kinase activities in mitotic cells. *Sci Signal*. 4:rs5.

Kim, Y., A.J. Holland, W. Lan, and D.W. Cleveland. 2010. Aurora kinases and protein phosphatase 1 mediate chromosome congression through regulation of CENP-E. *Cell*. 142:444-455.

Kinoshita, E., E. Kinoshita-Kikuta, K. Takiyama, and T. Koike. 2006. Phosphate-binding tag, a new tool to visualize phosphorylated proteins. *Mol Cell Proteomics*. 5:749-757.

Kotak, S., K. Afshar, C. Busso, and P. Gonczy. 2016. Aurora A kinase regulates proper spindle positioning in C. elegans and in human cells. *J Cell Sci*. 129:3015-3025.

Krauthammer, M., Y. Kong, B.H. Ha, P. Evans, A. Bacchiocchi, J.P. McCusker, E. Cheng, M.J. Davis, G. Goh, M. Choi, S. Ariyan, D. Narayan, K. Dutton-Regester, A. Capatana, E.C. Holman, M. Bosenberg, M. Sznol, H.M. Kluger, D.E. Brash, D.F. Stern, M.A. Materin, R.S. Lo, S. Mane, S. Ma, K.K. Kidd, N.K. Hayward, R.P. Lifton, J. Schlessinger, T.J. Boggon, and R. Halaban. 2012. Exome sequencing identifies recurrent somatic RAC1 mutations in melanoma. *Nat Genet*. 44:1006-1014.

Lampson, M.A., and I.M. Cheeseman. 2011. Sensing centromere tension: Aurora B and the regulation of kinetochore function. *Trends Cell Biol*. 21:133-140.

Levine, M.S., and A.J. Holland. 2018. The impact of mitotic errors on cell proliferation and tumorigenesis. *Genes Dev*. 32:620-638.

Liu, D., G. Vader, M.J. Vromans, M.A. Lampson, and S.M. Lens. 2009. Sensing chromosome bi-orientation by spatial separation of aurora B kinase from kinetochore substrates. *Science*. 323:1350-1353.

Long, A.F., D.B. Udy, and S. Dumont. 2017. Hec1 Tail Phosphorylation Differentially Regulates Mammalian Kinetochore Coupling to Polymerizing and Depolymerizing Microtubules. *Curr Biol*. 27:1692-1699 e1693.

Maciejowski, J., H. Drechsler, K. Grundner-Culemann, E.R. Ballister, J.A. Rodriguez-Rodriguez, V. Rodriguez-Bravo, M.J.K. Jones, E. Foley, M.A. Lampson, H. Daub, A.D. McAinsh, and P.V. Jallepalli. 2017. Mps1 Regulates Kinetochore-Microtubule Attachment Stability via the Ska Complex to Ensure Error-Free Chromosome Segregation. *Dev Cell*. 41:143-156 e146.

McCleland, M.L., R.D. Gardner, M.J. Kallio, J.R. Daum, G.J. Gorbsky, D.J. Burke, and P.T. Stukenberg. 2003. The highly conserved Ndc80 complex is required for kinetochore assembly, chromosome congression, and spindle checkpoint activity. *Genes Dev*. 17:101-114.

Musacchio, A. 2015. The Molecular Biology of Spindle Assembly Checkpoint Signaling Dynamics. *Curr Biol*. 25:R1002-1018.

Nijenhuis, W., E. von Castelmur, D. Littler, V. De Marco, E. Tromer, M. Vleugel, M.H. van Osch, B. Snel, A. Perrakis, and G.J. Kops. 2013. A TPR domain-containing N-terminal module of MPS1 is required for its kinetochore localization by Aurora B. *J Cell Biol*. 201:217-231.

Petrovic, A., J. Keller, Y. Liu, K. Overlack, J. John, Y.N. Dimitrova, S. Jenni, S. van Gerwen, P. Stege, S. Wohlgemuth, P. Rombaut, F. Herzog, S.C. Harrison, I.R. Vetter, and A. Musacchio. 2016. Structure of the MIS12 Complex and Molecular Basis of Its Interaction with CENP-C at Human Kinetochores. *Cell*. 167:1028-1040 e1015.

Petry, S. 2016. Mechanisms of Mitotic Spindle Assembly. *Annu Rev Biochem*. 85:659-683.

Polverino, F., F.D. Naso, I.A. Asteriti, V. Palmerini, D. Singh, D. Valente, A.W. Bird, A. Rosa, M. Mapelli, and G. Guarguaglini. 2021. The Aurora-A/TPX2 Axis Directs Spindle Orientation in Adherent Human Cells by Regulating NuMA and Microtubule Stability. *Curr Biol*. 31:658-667 e655.

Poser, E., R. Caous, U. Gruneberg, and F.A. Barr. 2019. Aurora A promotes chromosome congression by activating the condensin-dependent pool of KIF4A. *J Cell Biol*. 219.

Qian, J., M. Beullens, J. Huang, S. De Munter, B. Lesage, and M. Bollen. 2015. Cdk1 orders mitotic events through coordination of a chromosome-associated phosphatase switch. *Nat Commun*. 6:10215.

Rosas-Salvans, M., R. Sutanto, P. Suresh, and S. Dumont. 2022. The Astrin-SKAP complex reduces friction at the kinetochore-microtubule interface. *Curr Biol*.

Sanjana, N.E., O. Shalem, and F. Zhang. 2014. Improved vectors and genome-wide libraries for CRISPR screening. *Nat Methods*. 11:783-784.

Sarangapani, K.K., L.B. Koch, C.R. Nelson, C.L. Asbury, and S. Biggins. 2021. Kinetochore-bound Mps1 regulates kinetochore-microtubule attachments via Ndc80 phosphorylation. *J Cell Biol*. 220.

Schmidt, J.C., T. Kiyomitsu, T. Hori, C.B. Backer, T. Fukagawa, and I.M. Cheeseman. 2010. Aurora B kinase controls the targeting of the Astrin-SKAP complex to bioriented kinetochores. *J Cell Biol*. 191:269-280.

Sen, S., H. Zhou, and R.A. White. 1997. A putative serine/threonine kinase encoding gene BTAK on chromosome 20q13 is amplified and overexpressed in human breast cancer cell lines. *Oncogene*. 14:2195-2200.

Thein, K.H., J. Kleylein-Sohn, E.A. Nigg, and U. Gruneberg. 2007. Astrin is required for the maintenance of sister chromatid cohesion and centrosome integrity. *J Cell Biol*. 178:345-354.

Umbreit, N.T., D.R. Gestaut, J.F. Tien, B.S. Vollmar, T. Gonen, C.L. Asbury, and T.N. Davis. 2012. The Ndc80 kinetochore complex directly modulates microtubule dynamics. *Proc Natl Acad Sci U S A*. 109:16113-16118.

Wang, B., M. Wang, W. Zhang, T. Xiao, C.H. Chen, A. Wu, F. Wu, N. Traugh, X. Wang, Z. Li, S. Mei, Y. Cui, S. Shi, J.J. Lipp, M. Hinterndorfer, J. Zuber, M. Brown, W. Li, and X.S. Liu. 2019. Integrative analysis of pooled CRISPR genetic screens using MAGeCKFlute. *Nat Protoc*. 14:756-780.

Ye, A.A., J. Deretic, C.M. Hoel, A.W. Hinman, D. Cimini, J.P. Welburn, and T.J. Maresca. 2015. Aurora A Kinase Contributes to a Pole-Based Error Correction Pathway. *Curr Biol*. 25:1842-1851.

Yoo, T.Y., J.M. Choi, W. Conway, C.H. Yu, R.V. Pappu, and D.J. Needleman. 2018. Measuring NDC80 binding reveals the molecular basis of tension-dependent kinetochore-microtubule attachments. *Elife*. 7.

Zeng, K., R.N. Bastos, F.A. Barr, and U. Gruneberg. 2010. Protein phosphatase 6 regulates mitotic spindle formation by controlling the T-loop phosphorylation state of Aurora A bound to its activator TPX2. *J Cell Biol*. 191:1315-1332.

Zhang, C.Z., A. Spektor, H. Cornils, J.M. Francis, E.K. Jackson, S. Liu, M. Meyerson, and D. Pellman. 2015. Chromothripsis from DNA damage in micronuclei. *Nature*. 522:179-184.

Zhu, T., Z. Dou, B. Qin, C. Jin, X. Wang, L. Xu, Z. Wang, L. Zhu, F. Liu, X. Gao, Y. Ke, Z. Wang, F. Aikhionbare, C. Fu, X. Ding, and X. Yao. 2013. Phosphorylation of microtubule-binding protein Hec1 by mitotic kinase Aurora B specifies spindle checkpoint kinase Mps1 signaling at the kinetochore. *J Biol Chem*. 288:36149-36159.

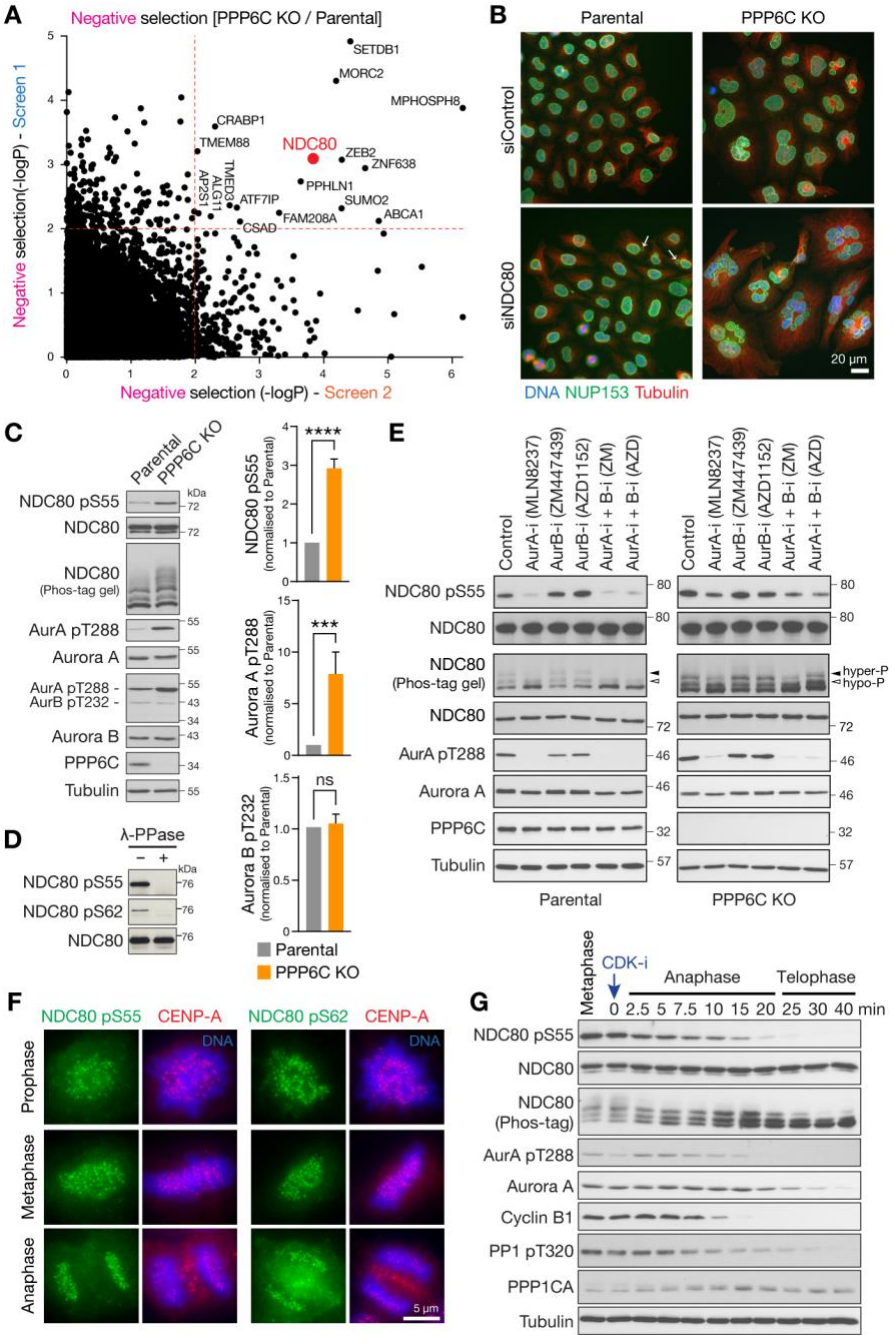

Fig. 1. Genome-wide CRISPR screening reveals synthetic growth defects between the catalytic subunit of PP6 and the kinetochore protein NDC80. (**A**) Genome-wide CRISPR screens were performed in parental and PPP6C KO eHAP cells for equal time of growth (Screen 1) or equal cell divisions (Screen 2). Significance (-logP) for negatively selected genes in PPP6C KO compared to the parental background is plotted for screen 1 against screen 2. Dotted red lines mark p = 0.01 significance level. NDC80 is highlighted. (**B**) Parental and PPP6C KO cells depleted of NDC80 were stained for DNA, tubulin and the nuclear pore marker NUP153. Arrows mark micronuclei in NDC80 depleted parental cells. (**C**) Mitotic lysates of parental and PPP6C KO HeLa cells were blotted for the proteins listed in the figure. Overall NDC80 phosphorylation was monitored using a Phos-tag gel. Relative levels of NDC80 S55 phosphorylation, active Aurora A (pT288) and active Aurora B (pT232) were measured (mean ± SEM). (**D**) Mitotic

HeLa cell lysates mock (-) or lambda-phosphatase treated (+λ-PPase) were blotted for NDC80, NDC80 pS55 and pS62. (**E**) Mitotic lysates of parental and PPP6C KO HeLa cells treated with Aurora A (AurA-i) and B (AurB-i) kinase inhibitors in the combinations shown were blotted for the proteins listed in the figure. (**F**) HeLa cells in different stage of mitosis stained for NDC80 pS55 or pS62, DNA and CENP-A. (**G**) HeLa cells in mitosis were treated with CDK-inhibitor (CDK-i) to promote entry into anaphase and mitotic exit. NDC80 phosphorylation was followed using NDC80 pS55 and Phos-tag gels. Mitotic exit was confirmed by blotting for cyclin B, the inhibitory pT320 modification of PP1, and active Aurora A pT288.

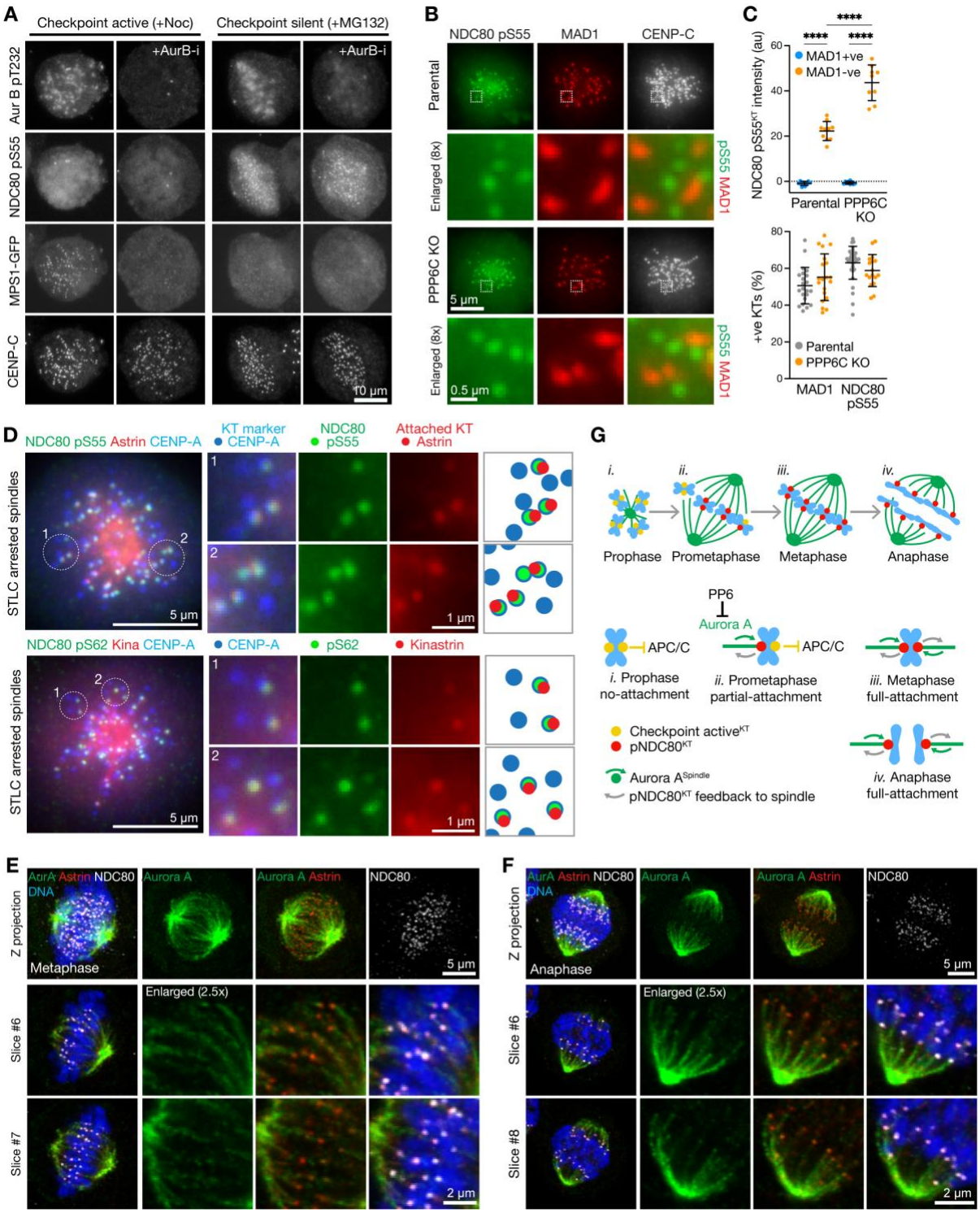

Fig. 2. NDC80 is phosphorylated by Aurora A at microtubule-attached kinetochores. (**A**) HeLa MPS1-GFP^{CRISPR} cells arrested in mitosis with either nocodazole or the proteasome inhibitor MG132 were left untreated or treated with Aurora B inhibitor (AurB-i). Cells were stained for active Aurora B pT232, phosphorylated NDC80 pS55, and the kinetochore marker CENP-C. (**B**) Parental and PPP6C KO HeLa cells arrested with STLC to create monoastral spindles with a mixture checkpoint active and silent kinetochores states were stained for MAD1, NDC80 pS55, CENP-C and DNA. (**C**) NDC80 pS55 was measured at MAD1 positive (+ve) and

negative (-ve) kinetochores (mean ± SD), and the proportion of MAD1 positive kinetochores was determined for parental and PPP6C KO HeLa cells. (**D**) Hela cells arrested with STLC were stained for NDC80 pS55, astrin, CENP-A and DNA or NDC80 pS62, kinastrin, CENP-A and DNA. Enlarged region and schematics show the relationship of NDC80 pS55 or pS62 and astrin or kinastrin staining relative to the centromere and kinetochore marker CENP-A. (**E**) Confocal images of metaphase or (**F**) anaphase HeLa cells stained for Aurora A, astrin, NDC80 and DNA. Enlarged region show the proximity of astrin-positive kinetochores to Aurora A spindle fibers in metaphase and anaphase. (**G**) Schematic showing the relationship of Aurora A bearing spindle fibers (green, green arrow), NDC80 phosphorylation (red) and spindle checkpoint signaling (yellow) at kinetochores during different stages of spindle formation. PP6 limits Aurora A activity towards NDC80. NDC80 phosphorylation alters the properties of kinetochores (grey arrow), and movement on microtubules allowing spindles to.

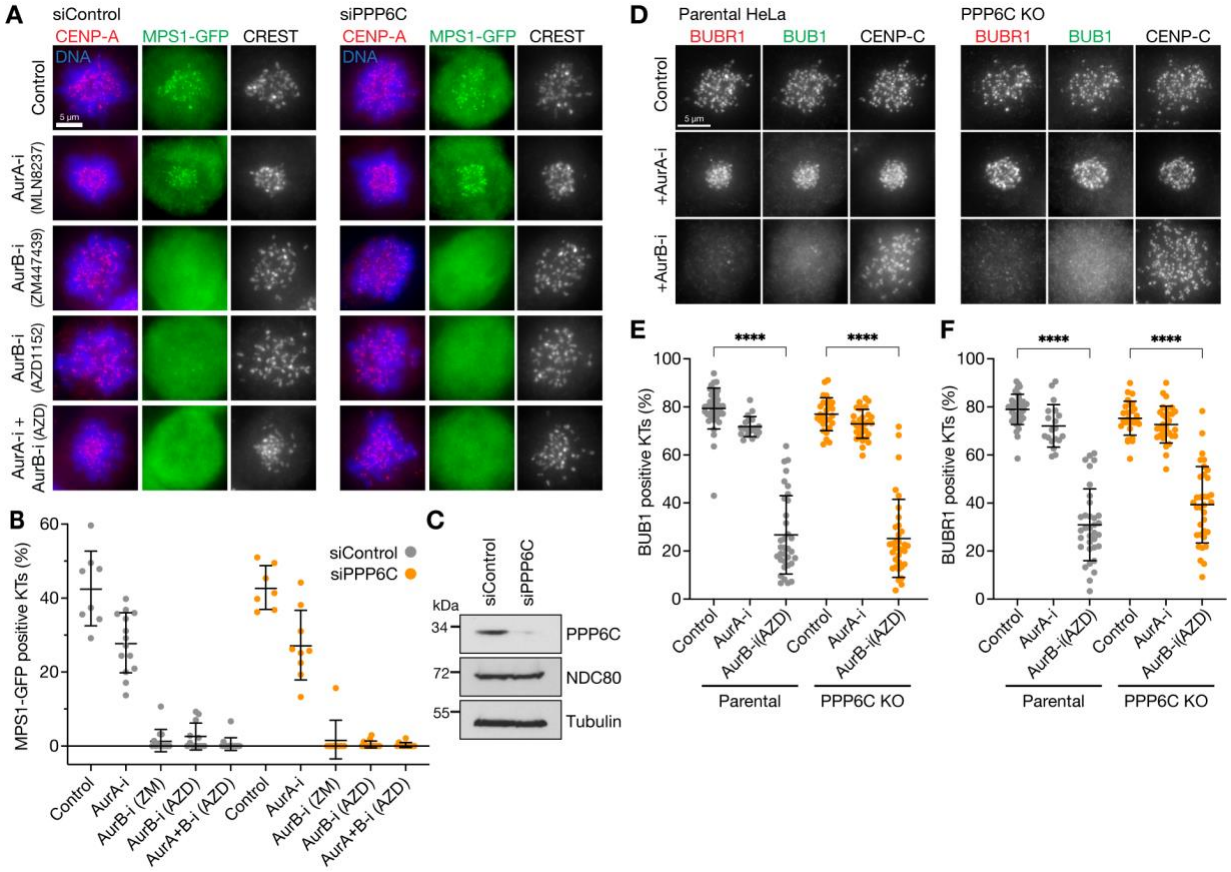

Fig. 3. MPS1 recruitment and spindle checkpoint signaling is insensitive to Aurora A activity in parental and PPP6C KO cells. (**A**) Control and PPP6C-depleted HeLa MPS1-GFP^{CRISPR} cells arrested with STLC to form monoastral spindle were treated with Aurora A (AurA-i) and Aurora B (AurB-i) inhibitors alone or in combination and then stained for DNA, CREST and CENP-A. (**B**) The number of MPS1-GFP positive kinetochores in control and Aurora kinase inhibited parental and PPP6C-depleted cells (mean ± SD). (**C**) Western blot to confirm depletion of PPP6C. (**D**) Parental and PPP6C KO HeLa cells were treated with either Aurora A or Aurora B inhibitors and stained for DNA, the kinetochore protein CENP-C, and spindle checkpoint proteins BUB1 and BUBR1. (**E**) The number of BUB1 or (**F**) BUBR1 positive kinetochores in parental and PPP6C KO cells treated with Aurora kinase inhibitors (mean ± SD).

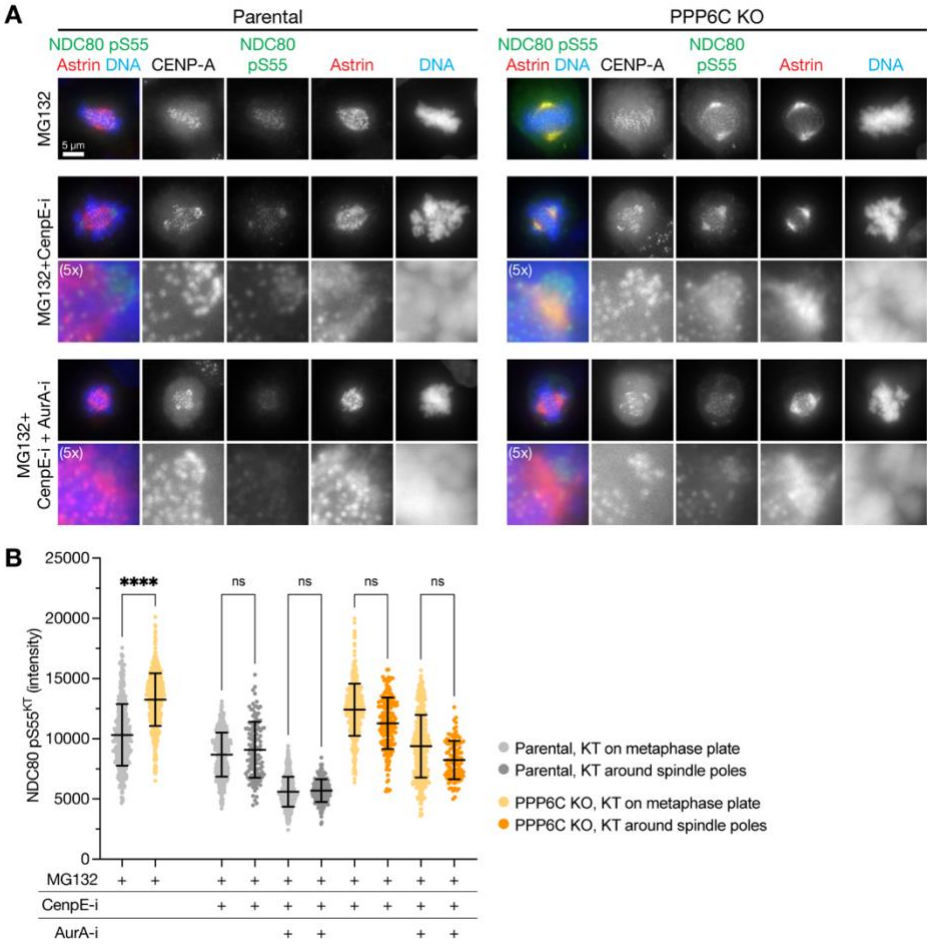

Fig. 4. NDC80 phosphorylation is elevated in PPP6C KO cells, independent of the spatial position of chromosomes within the mitotic spindle. (**A**) Parental and PPP6C KO HeLa cells were arrested in metaphase with MG132 with aligned chromosomes, with MG132 and CENP-E (CenpE-i) inhibitor to trap some chromosomes at the spindle poles, or with MG132, CENP-E and Aurora A (AurA-i) inhibitors. Cells were stained for NDC80 pS55, astrin, CENP-A, and DNA. Enlarged panels for CENP-E inhibitor conditions show kinetochores close to spindle poles. (**B**) NDC80 pS55 intensity (mean ± SD) at metaphase aligned chromosomes (MG132) and chromosomes trapped at spindle poles (MG132+CenpE-i). Aurora A inhibitor was used to confirm NDC80 pS55 signal was dependent on Aurora A activity for aligned and trapped chromosomes.

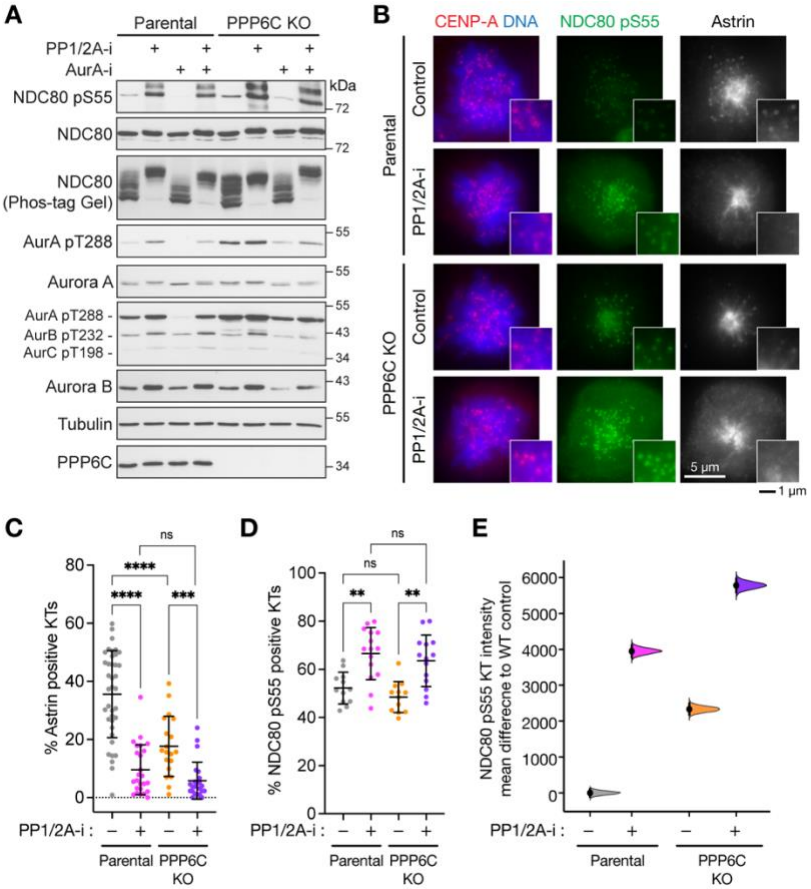

Fig. 5. NDC80 phosphorylation is limited by counteracting P1/PP2A phosphatases. (**A**) Mitotic lysates of parental and PPP6C KO HeLa cells treated with Aurora A (AurA-i) and phosphatase (calyculin, PP1/2A-i) inhibitors in the combinations shown were blotted for the proteins listed in the figure. Overall NDC80 phosphorylation was monitored using a Phos-tag gel. (**B**) Parental and PPP6C KO cell lines were treated with STLC to arrest cells in mitosis in the absence (Control) and presence of PP1/2A-i. (**C**) The number of astrin or (**D**) NDC80 pS55 positive kinetochores was measured for the different conditions (mean ± SD). (**E**) Level of NDC80 pS55 signal was measured for the different conditions. Each mean difference is depicted as a dot. Each 95% confidence interval is indicated by the ends of the vertical error bars; the confidence interval is bias-corrected and accelerated.

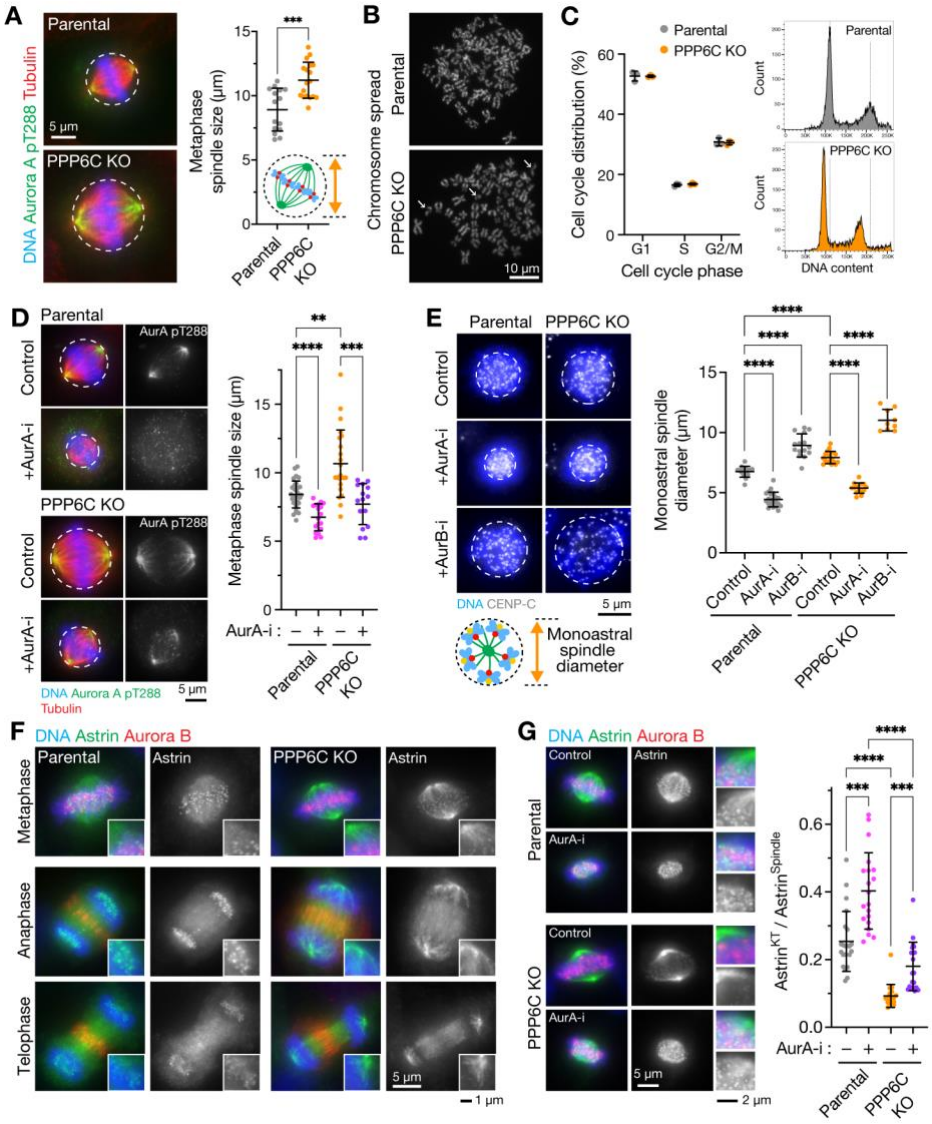

Fig. 6. PP6 and Aurora A regulate the size of the mitotic spindle. (**A**) Metaphase spindle size (mean ± SD) was measured in parental and PPP6C KO HeLa cell lines. (**B**) Mitotic chromosome spreads from parental and PPP6C KO HeLa cell lines. Arrows indicate broken or unpaired chromosomes. (**C**) Flow cytometry was used to measure cell cycle distribution (mean ± SD) and ploidy of parental and PPP6C KO HeLa cells. (**D**) Metaphase spindle size (mean ± SD) was measured in parental and PPP6C KO HeLa cell lines in the presence (+) or absence (-) of Aurora A inhibitor (AurA-i). (**E**) Parental and PPP6C KO cell lines were treated with STLC to arrest cells in mitosis in the absence (Control) and presence of Aurora A (AurA-i) or Aurora B (AurB-i) inhibitors. Monoastral spindle diameter (mean ± SD) was measured for the different conditions. (**F**) Parental and PPP6C KO cells stained for the kinetochore-associated protein astrin, Aurora B and DNA are shown at different stages of mitosis. (**G**) Parental and PPP6C KO cell lines were treated with STLC to arrest cells in mitosis in the absence (Control) and presence of Aurora A (AurA-i) inhibitor. Astrin distribution at kinetochores and spindle poles was measured and expressed as a ratio ($Astrin^{KT}/Astrin^{Spindle}$, mean ± SD) for the different conditions.

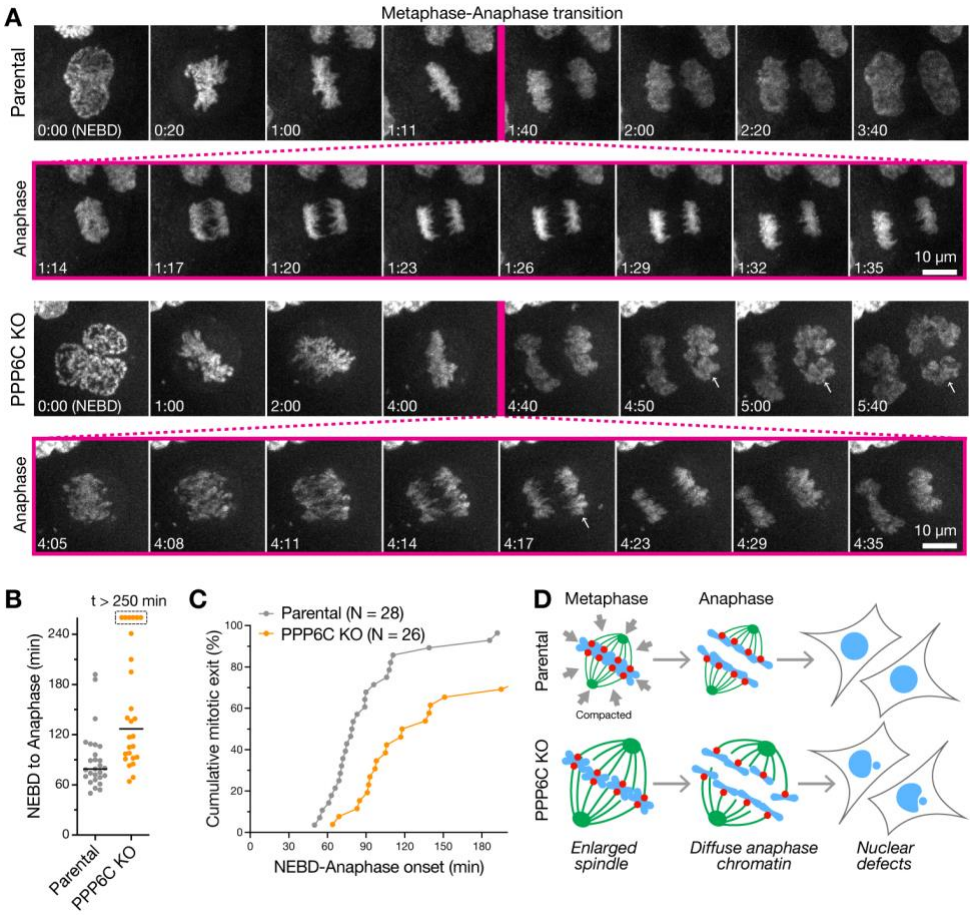

Fig. 7. Enlarged metaphase spindle size results in defective chromosome segregation and nuclear morphology defects. (**A**) Time-lapse imaging of DNA segregation in parental and PPP6C KO cells. Nuclear envelope breakdown (NEBD) was taken as the start of mitosis. Anaphase is shown with higher time resolution with arrows to mark anaphase spindle defects in PPP6C KO cells. Arrows indicate chromosomes escaping the anaphase spindle. (**B**) Mitotic progression from NEBD to anaphase onset (the line marks the median value) and (**C**) cumulative mitotic index in parental and PPP6C KO cells. PPP6C KO cells show extended mitosis and delayed mitotic exit. (D) A schematic outlining how the enlarged spindles in PPP6C KO cells fail to maintain a compact array of chromosomes in anaphase. Escaped chromosomes then form micronuclei and other nuclear shape defects.

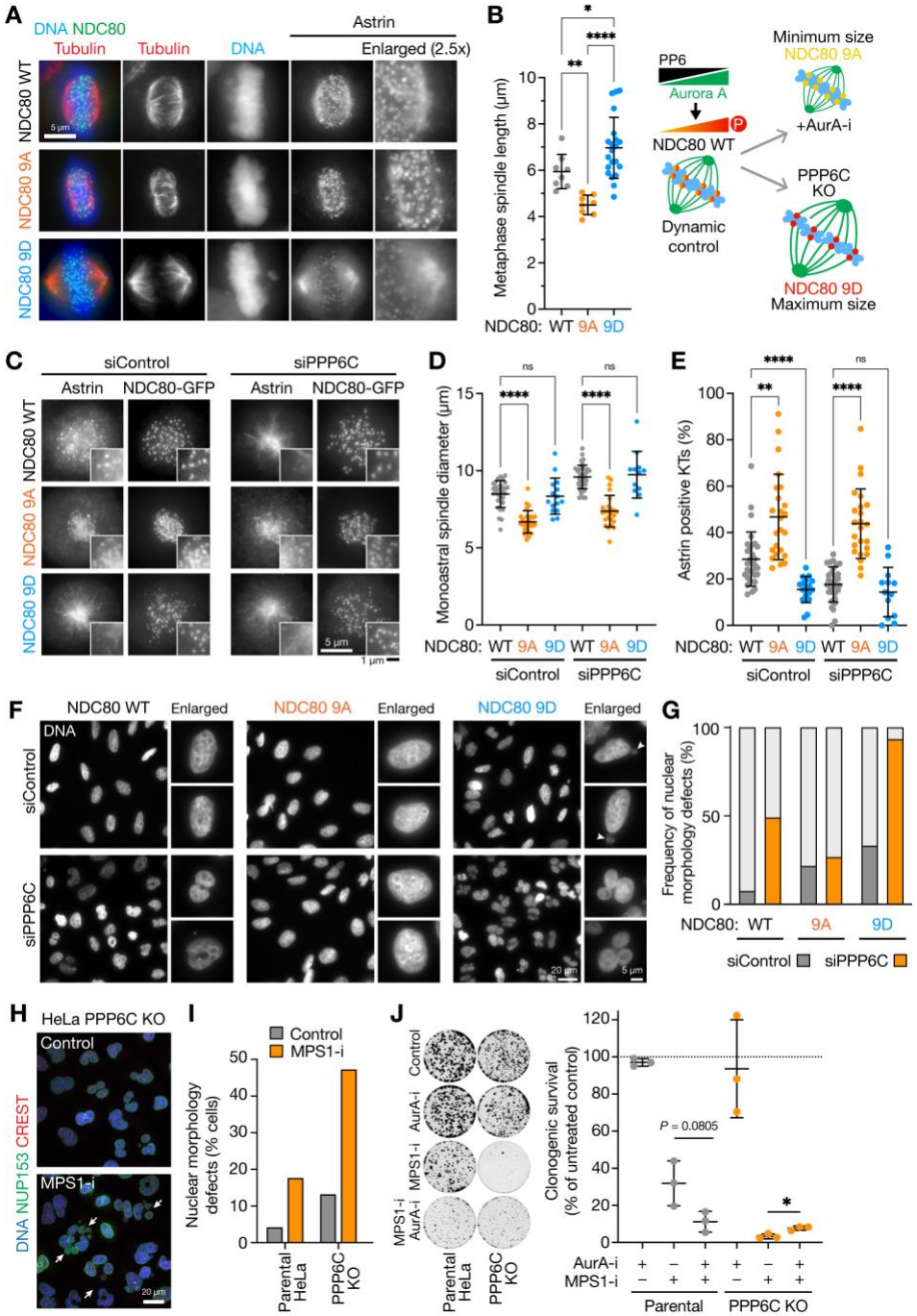

Fig. 8. NDC80 phospho-mutants rescue the spindle size and micronucleation defects seen in PP6 deficient cells. (**A**) HeLa FlpIn T-REx NDC80-GFP wild-type (WT), 9A and 9D cells depleted of endogenous NDC80 were stained for tubulin and DNA. Enlarged regions show the presence or loss of astrin staining at kinetochores in mitotic cells. (**B**) Metaphase spindle length (mean ± SD) was measured and a schematic of the effects on spindle size is shown to the right. (**C**) HeLa FlpIn T-REx NDC80-GFP wild-type (WT), 9A and 9D cells transfected with control or PPP6C siRNA for 72h were treated with STLC to create monopolar spindles and stained for astrin. Enlarged regions show the presence or loss of astrin staining at kinetochores. (**D**)

Monoastral spindle diameter and (**E**) the number of astrin-positive kinetochores (mean ± SD) were measured for the conditions shown. (**F**) HeLa FlpIn T-REx NDC80-GFP WT, 9A and 9D cells treated with control or PPP6C siRNA for 72h were stained for DNA, and (**G**) the frequency of cells with nuclear morphology defects scored. (**H**) Parental and PPP6C KO cells treated with MPS1 inhibitor (MPS1-i) for 48h were stained for DNA, NUP153, and the centromere marker CREST, and (**I**) the frequency of cells with nuclear morphology defects scored. (**J**) Clonogenic survival assays for parental and PPP6C KO cells treated with 10 nM Aurora A (AurA-i) and 1 µM MPS1 (MPS1-i) inhibitors alone or in combination (mean ± SD). Example plates for clonogenic survival assays are shown to the left of the graphed data.

Supplementary Material for:

Protein phosphatase 6 regulates mitotic spindle size by limiting Aurora A phosphorylation of NDC80

Tomoaki Sobajima, Katarzyna M. Kowalczyk, Stefanos Skylakakis, Daniel Hayward, Luke J. Fulcher, Colette Neary, Caleb Batley, Emile Roberts, Samvid Kurlekar, Ulrike Gruneberg, Francis A. Barr

Correspondence to: francis.barr@bioch.ox.ac.uk

Figs. S1 to S10

Table S1. Genome-wide CRISPR screening summary data tables

Table S2. List of commercial and custom siRNA duplexes

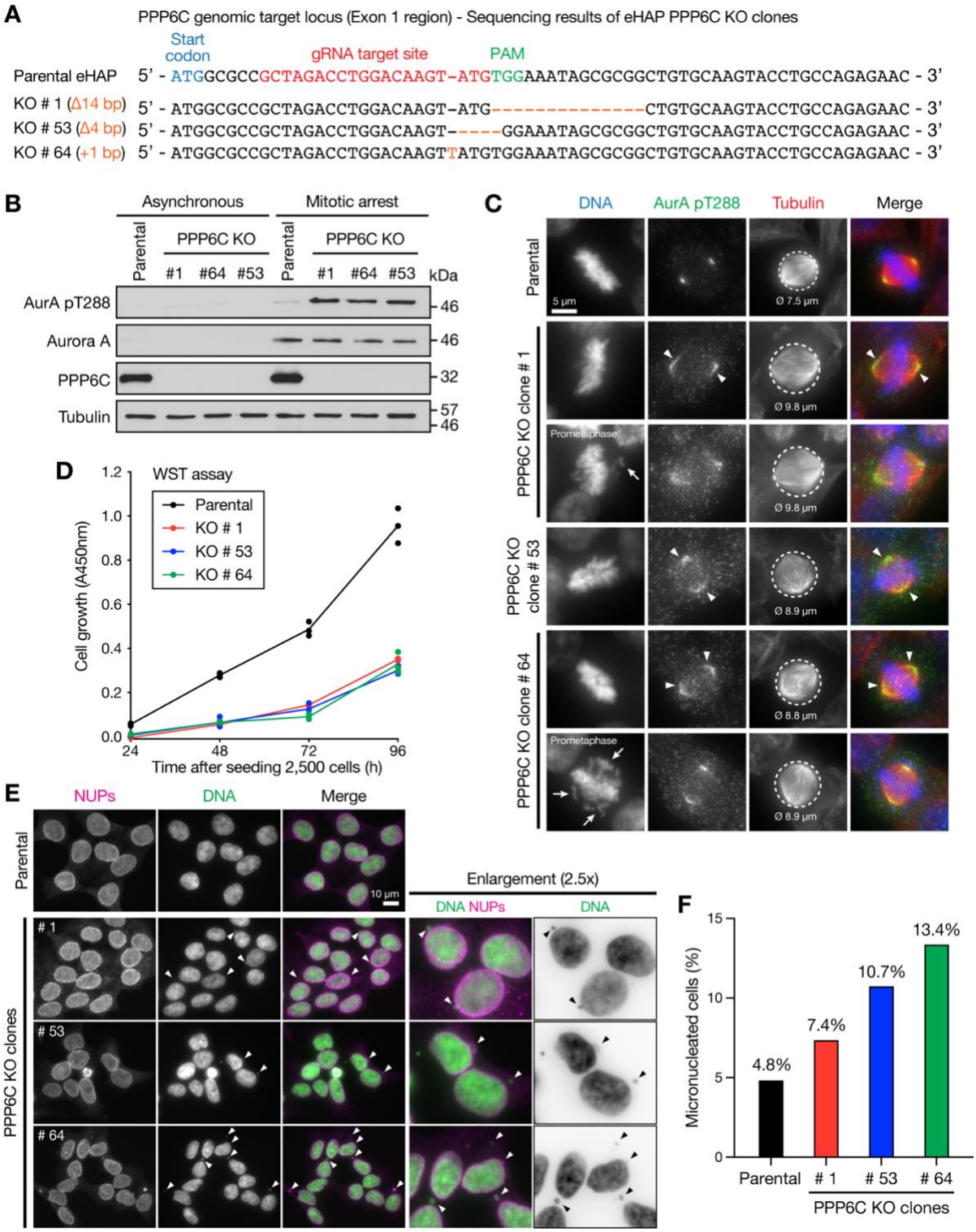

Fig. S1. Characterization of PPP6C knockout eHAP cell lines. (**A**) DNA sequence of the PPP6C genomic locus showing the sequence of 3 candidate PPP6C KO alleles. (**B**) Western blot of parental eHAP and candidate PPP6C KO alleles showing loss of PPP6C protein and elevation of active Aurora A pT288. (**C**) Parental eHAP and PPP6C KO cells stained for Aurora A pT288, tubulin, and DNA. Arrowheads mark spread of active Aurora A on the mitotic spindle, and arrows indicate chromosome missegregation. (**D**) Growth rate of parental eHAP and PPP6C KO

cell lines. (**E**) Parental eHAP and PPP6C KO cells stained for nuclear pore proteins (NUPs) and DNA. Arrowheads indicate micronuclei. (**F**) Frequency of micronucleation in parental and PPP6C KO eHAP clones.

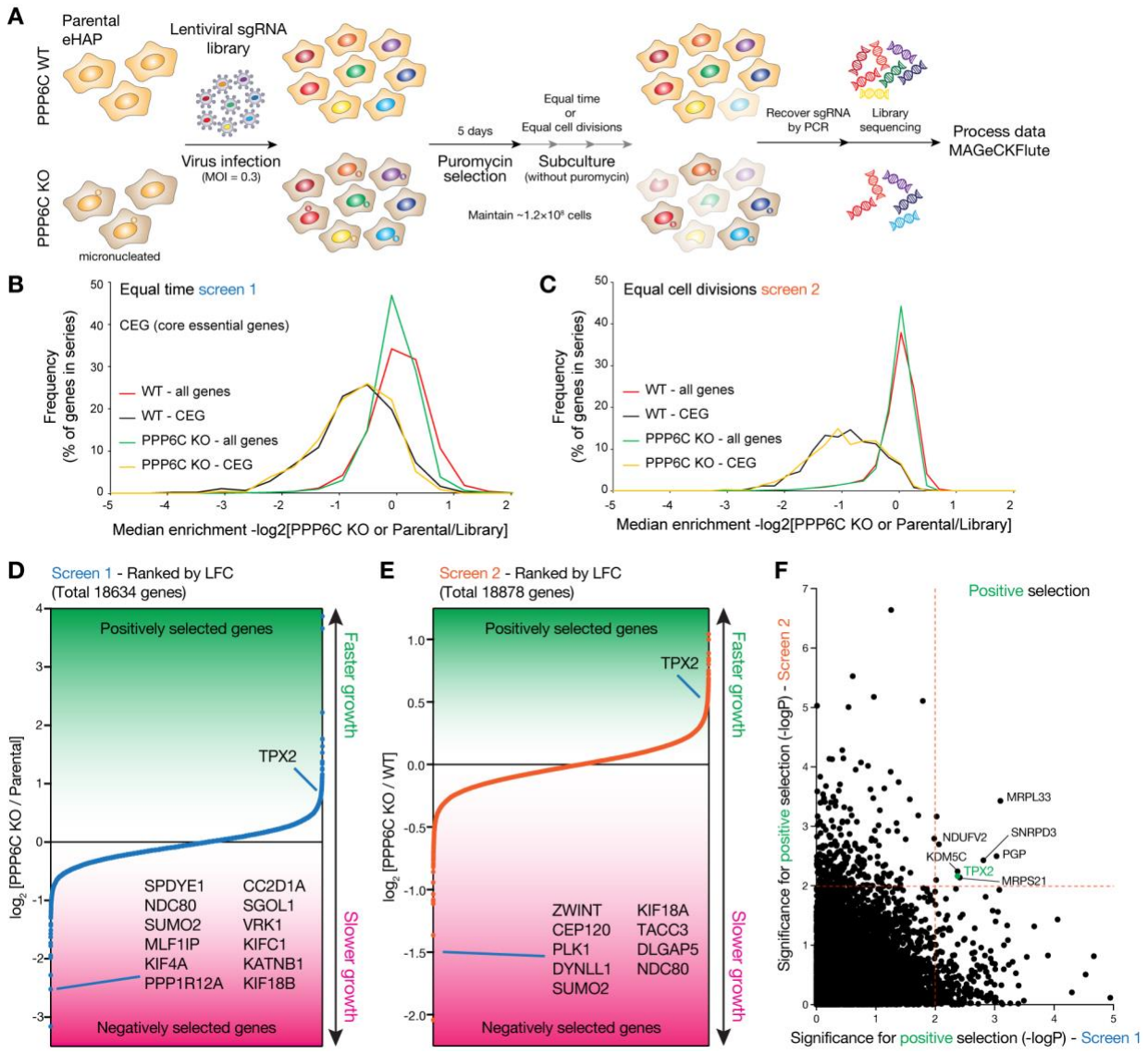

Fig. S2. Genome-wide haploid genomic screen for synthetic growth defects with PPP6C. (**A**) Workflow for genome-wide CRISPR knockout screens and data analysis. (**B**) Frequency plot of median enrichment of all genes and a selected set of core essential genes for the equal growth time screen 1 and (**C**) equal cell divisions screen 2. Selection for essential genes was observed in both parental and PPP6C KO cells. (**D**) Genes ranked by relative log-fold change (LFC) [PPP6C KO/ parental] from negative to positive for the equal growth time screen 1 and (**E**) equal cell divisions screen 2. Positively and negatively selected genes filtered for p<0.01 are listed inside the plots. (**E**) Significance (-logP) for positively selected genes is plotted for screen 1 against screen 2. Dotted red lines mark p = 0.01 significance level.

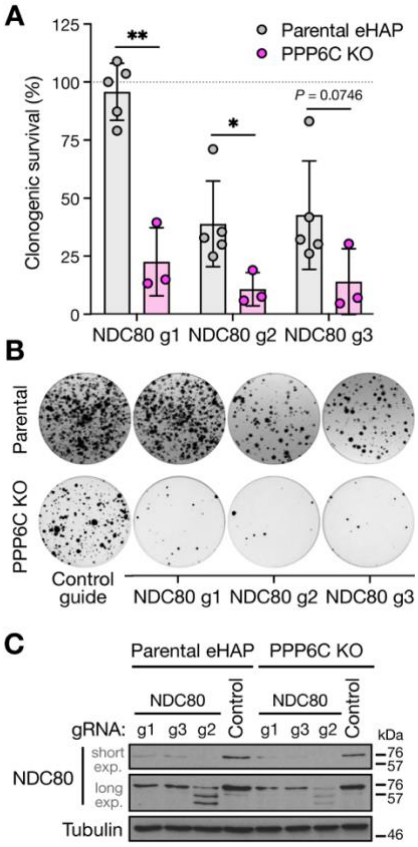

Fig. S3. Validation of NDC80 synthetic lethality with PPP6C in eHAP. (**A**) Clonogenic survival assays for 3 gRNA sequences targeting NDC80 (mean ± SD). (**B**) Example images of clonogenic survival assays. (**C**) Western blot validation of NDC80 depletion by the g1-g3 gRNA sequences. Note g2 results in reduced expression and a ladder of truncated NDC80 protein species.

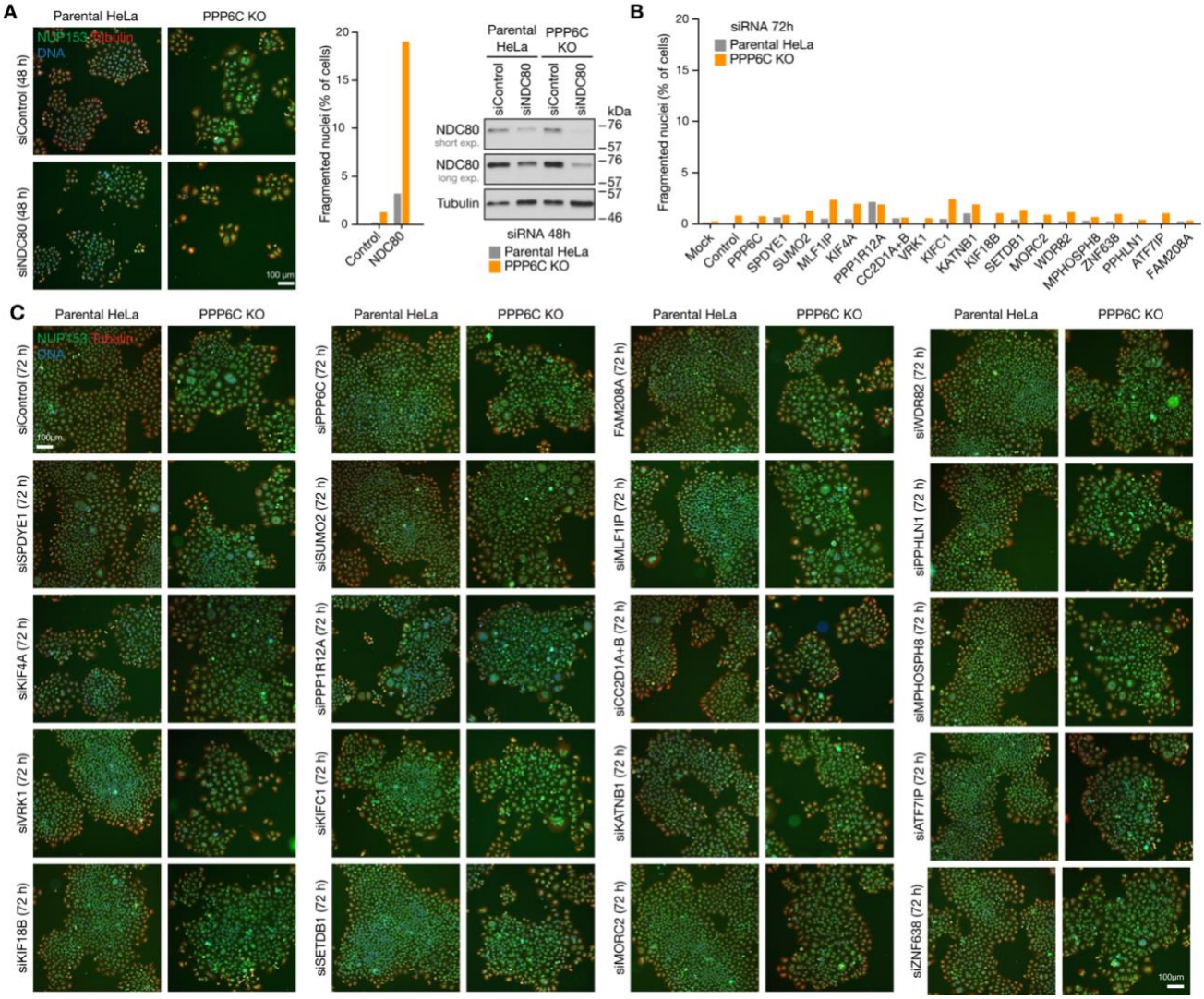

Fig. S4. Nuclear morphology assay of significant candidates from PPP6C synthetic growth defect screen. (**A**) Parental and PPP6C KO HeLa cells treated with control and NDC80 siRNA for 48h were stained for NUP153, tubulin, and DNA and the proportion of morphologically abnormal nuclei plotted in the graph. Western blot confirms depletion of NDC80. (**B**) Parental and PPP6C KO HeLa cells were treated for 72h with siRNA for the indicated candidate genes identified by genome wide synthetic lethality with PPP6C KO. The proportion of morphologically abnormal nuclei is plotted in the graph with (**C**) representative images of the cells.

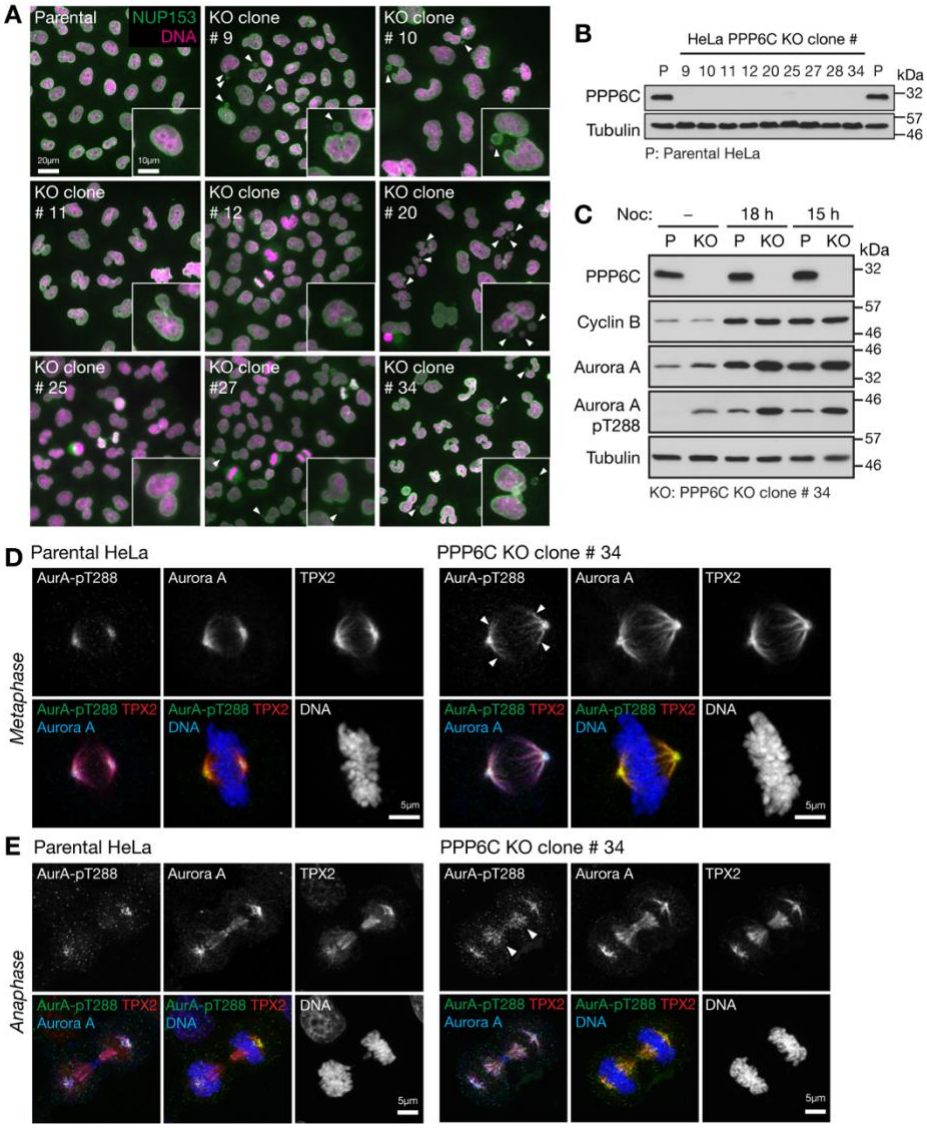

Fig. S5. Characterization of PPP6C knockout HeLa cell lines. (**A**). Parental and candidate PPP6C KO cell lines were stained for DNA and NUP153, arrowheads indicate micronuclei or nuclear morphology defects, or (**B**) western blotted for tubulin and PPP6C. (**C**) Parental (P) and PPP6C KO clone # 34 in asynchronous culture or arrested in mitosis for 15h or 18h with nocodazole were blotted for cyclin B and the activating pT288 phosphorylation on Aurora A. (**D**) Metaphase and (**E**) anaphase parental and PPP6C KO HeLa cells stained for Aurora A, the Aurora A activating protein TPX2, active Aurora A pT288, and DNA. Arrowheads indicate the spread of active Aurora A on metaphase and anaphase spindles in PPP6C KO cells. Note the enlarged metaphase plate in PPP6C KO cells.

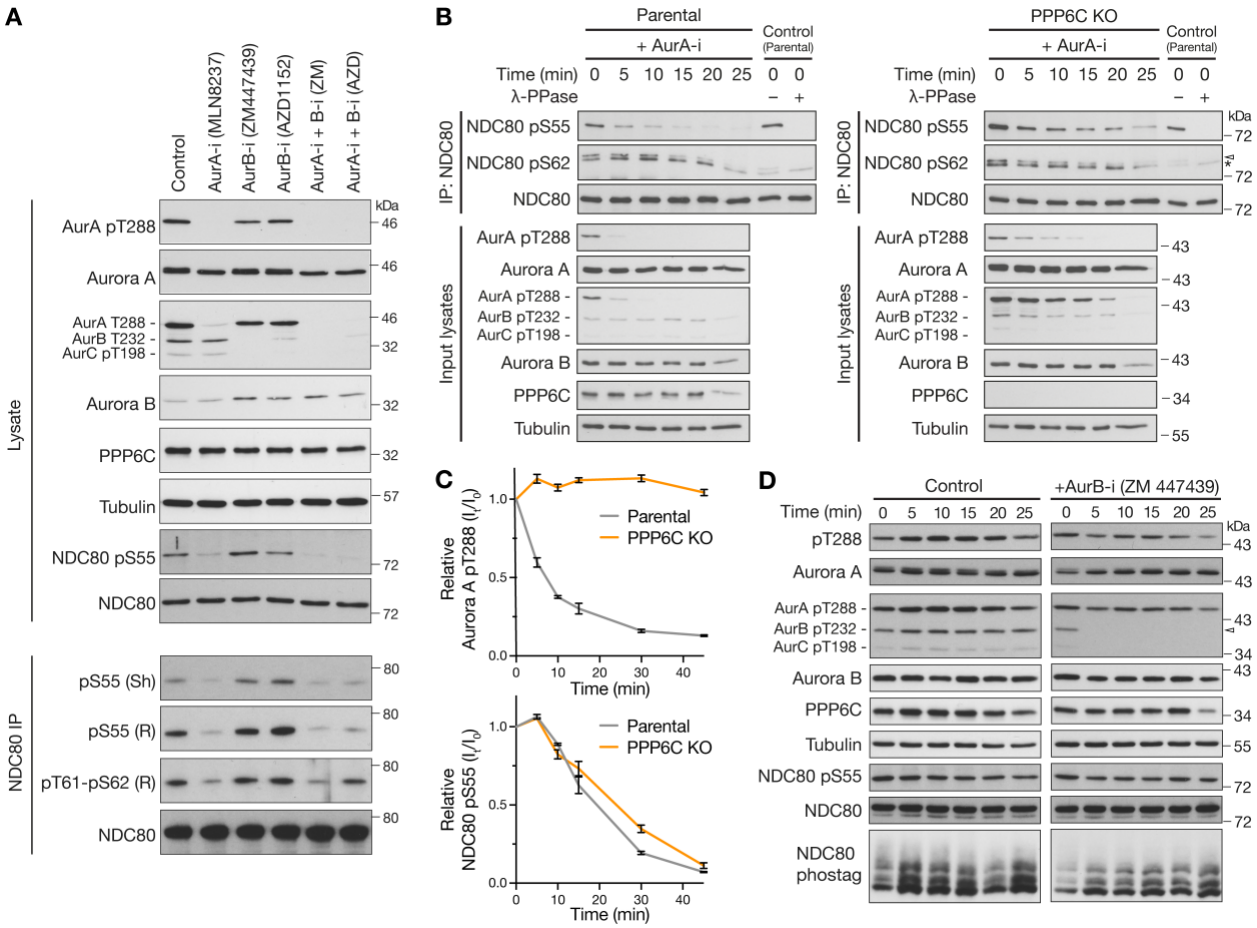

Fig. S6. PP6 regulates Aurora A and is not an NDC80 counteracting phosphatase. (**A**) HeLa cells were arrested in mitosis with nocodazole and then released to allow mitotic spindle formation in the presence of Aurora A and Aurora B kinase inhibitors as indicated. Cell lysates were prepared and NDC80 isolated by immune precipitation (NDC80 IP). Lysates and IP samples were western blotted with antibodies to Aurora A and B, activated Aurora A pT288, a pan-phospho-Aurora antibody detecting pT288 and pT232, NDC80, NDC80 pS55 and pT61-pS62 (rabbit, R; sheep, Sh). (**B**) Parental and PPP6C KO cells were arrested in mitosis with nocodazole and then released to allow mitotic spindle formation in the presence of Aurora A inhibitor (AurA-i) for the times indicated. Cell lysates were prepared and NDC80 isolated by immune precipitation (NDC80 IP). Lysates and IP samples were western blotted with antibodies to Aurora A and B, activated Aurora A pT288, a pan-Aurora antibody detecting pT288 and pT232, NDC80 pS55 and pS62. (**C**) Aurora A pT288 and NDC80 pS55 dephosphorylation in parental and PPP6C KO cells. Aurora A pT288 is stabilized following Aurora A inhibition in PPP6C KO cells (mean ± SEM). (**D**) HeLa cells were arrested in mitosis with nocodazole and then released to allow mitotic spindle formation in the presence of Aurora B inhibitors (AurB-i) for the times indicated. Cell lysates were prepared and western blotted with antibodies to Aurora A and B, activated Aurora A pT288, a pan-phospho-Aurora antibody detecting pT288 and pT232, NDC80 pS55. Both Aurora A pT288 and NDC80 pS55 were stable under these conditions.

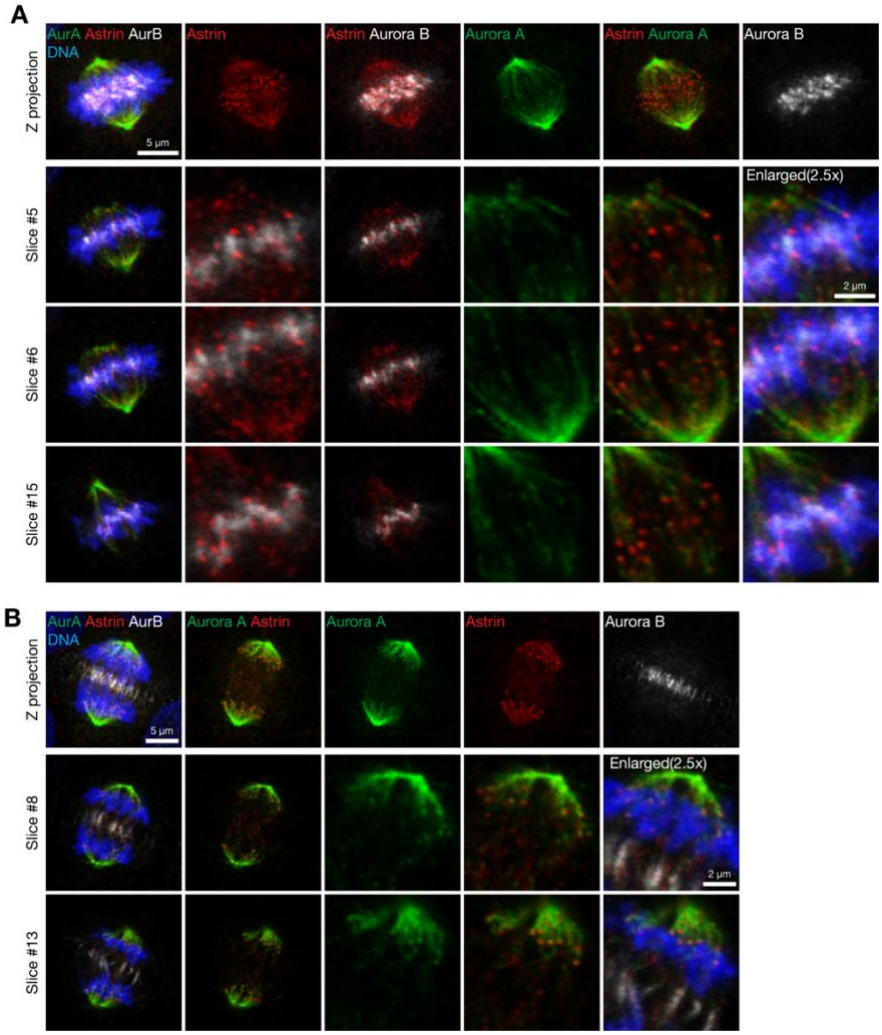

Fig. S7. Aurora B localization in metaphase and anaphase. (**A**) Confocal images of metaphase or (**B**) anaphase HeLa cells stained for Aurora B, Aurora A, astrin, and DNA. Enlarged regions show the proximity of astrin-positive kinetochores to Aurora A spindle fibres in both metaphase and anaphase. In metaphase, Aurora B flanks NDC80 and astrin-positive kinetochores. In anaphase, Aurora B relocates to the central spindle and spatially segregated from NDC80 and astrin-positive kinetochores.

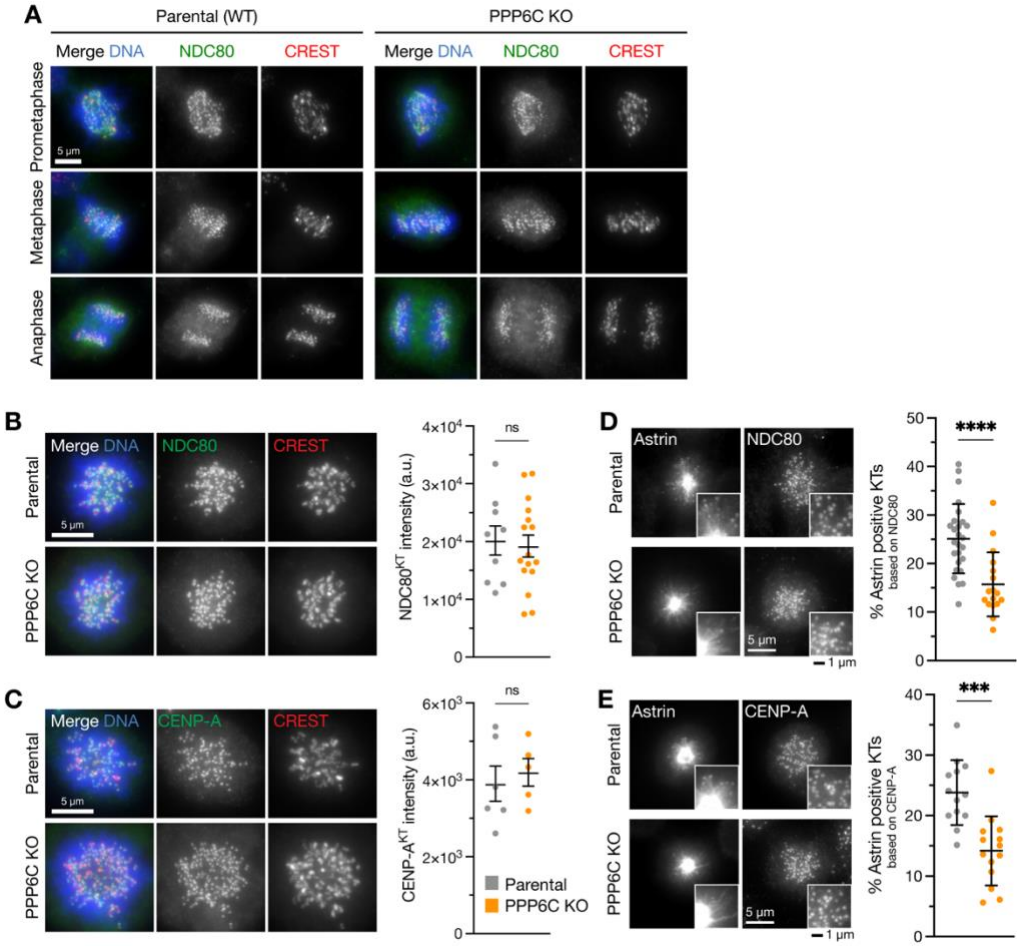

Fig. S8. Astrin is lost from kinetochores in PPP6C KO cells. (**A**) Parental and PPP6C KO cells stained for the kinetochore-protein NDC80, centromere marker CREST, and DNA are shown at different stages of mitosis. (**B**) Parental and PPP6C KO cells treated with STLC to create monopolar spindles stained for CREST, DNA, NDC80 or (**C**) CENP-A were used to measure NDC80 or CENP-A intensity at kinetochores (mean ± SEM). (**D**) STLC-treated parental and PPP6C KO cells were stained for astrin, DNA, NDC80 or CENP-A. Astrin-positive kinetochores (mean ± SD) were defined by either NDC80 or (**E**) CENP-A.

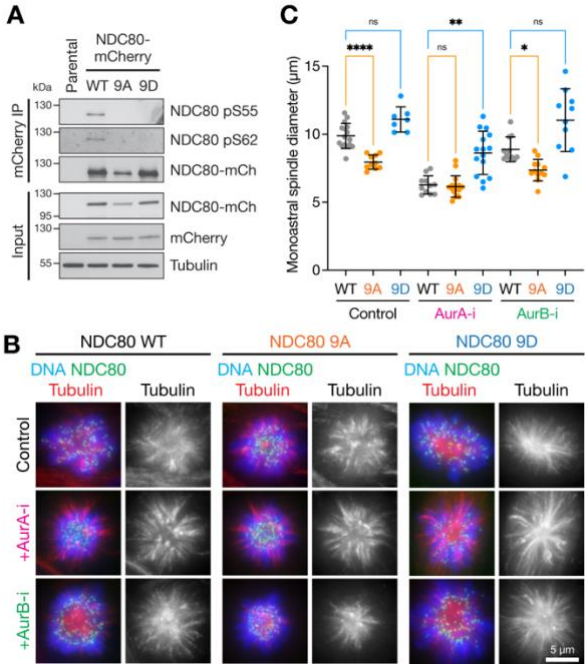

Fig. S9. NDC80-9A expression or Aurora A inhibition result in reduced monopolar spindle size. (**A**) HeLa FlpIn T-REx NDC80-GFP wild-type (WT), NDC80-9A and NDC80-9D cells in mitosis were western blotted with the NDC80 pS55 and pS62 antibodies to confirm the expected pattern of NDC80 phosphorylation. (**B**) HeLa FlpIn T-REx GFP-NDC80 wild-type (WT), 9A and 9D cells arrested with STLC to create monopolar spindles were treated with Aurora A or Aurora B inhibitors and stained for DNA and tubulin. (**C**) Monoastral spindle diameter (mean ± SD) was measured for the conditions shown.

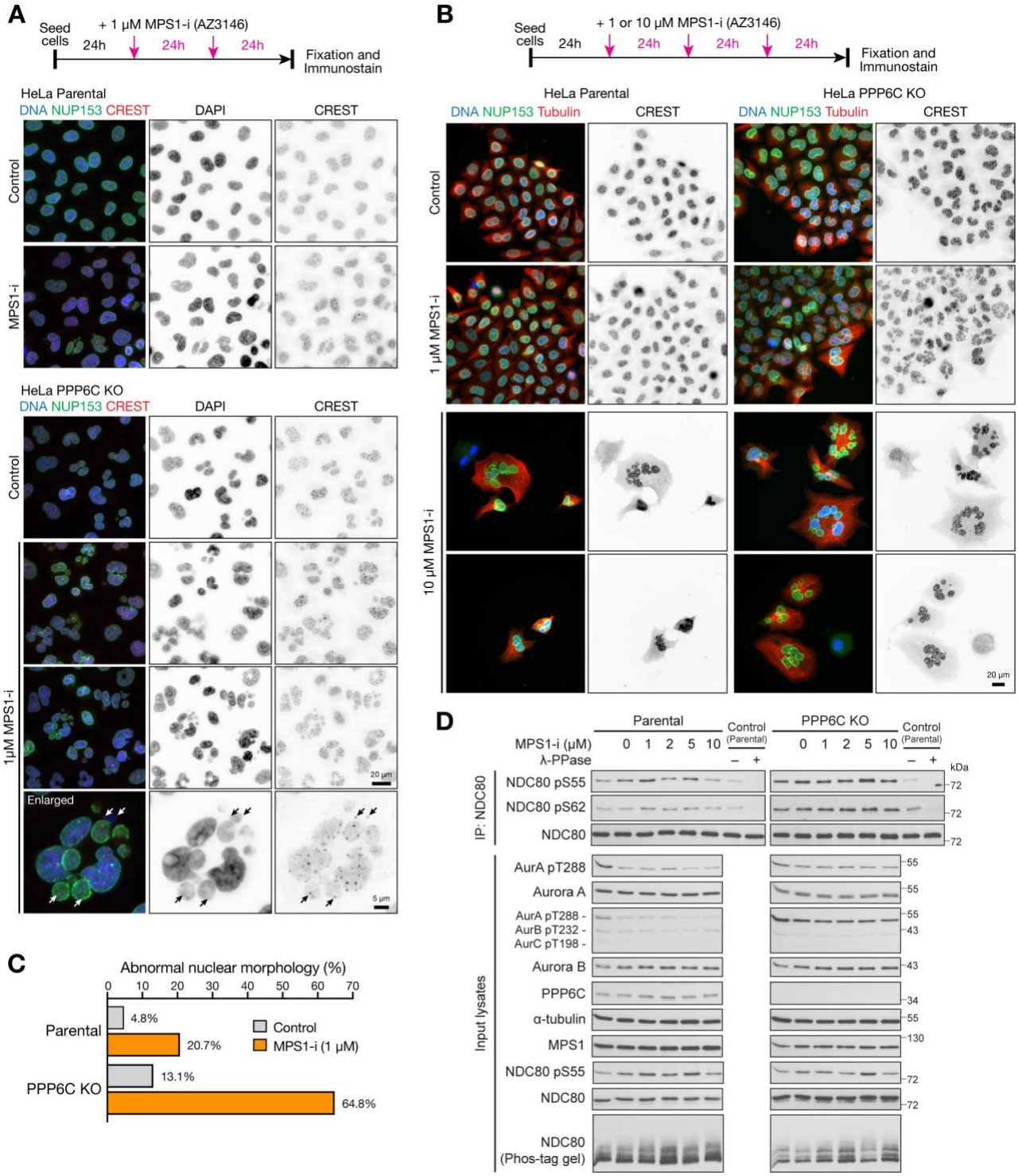

Fig. S10. Spindle checkpoint signaling is required for the viability of PPP6C KO cells. (**A**) Parental and PPP6C KO cells treated with 1 μM MPS1 inhibitor (MPS1-i) for 48h or (**B**) 1 or 10 μM MPS1-I for 72h were stained for DNA, NUP153, and the centromere marker CREST. (**C**) The frequency of cells with nuclear morphology defects following 72h of 1 μM MPS1-i. (**D**) Mitotic lysates of parental and PPP6C KO HeLa cells treated with MPS1 inhibitor (MPS1-i) were blotted for the proteins listed in the figure. A sample of control lysate, or control lysate treated with lambda-phosphatase (λ-PPase) were used as positive and negative controls.